Přírodovědecká fakulta Univerzity Palackého
v Olomouci

Společná laboratoř optiky

Experimentální kvantové zpracování informace s fotonovými páry

DIZERTAČNÍ PRÁCE

Karel Lemr

školitel:
doc. Mgr. Jan Soubusta, Ph.D.

FACULTY OF SCIENCE, PALACKÝ UNIVERSITY
IN OLOMOUC

JOINT LABORATORY OF OPTICS

Experimental quantum information processing with photon pairs

PH.D. THESIS

Karel Lemr

supervisor:
doc. Mgr. Jan Soubusta, Ph.D.

OLOMOUC   FEBRUARY 2012

Bibliographic details

Title	Experimental quantum information processing with photon pairs
Nadpis	Experimentální kvantové zpracování informace s fotonovými páry
Titre	Traitement de l'information quantique expérimental avec des pairs de photons
Type	Ph.D. thesis
Author	Karel Lemr
Supervisor	doc. Mgr. Jan Soubusta, Ph.D.
University	Palacký University in Olomouc
Study program	P1703 Physics,
	1701V029 Optics and Optoelectronics
Department	Joint Laboratory of Optics
Language	English
Year	2012
Pages	93
Available at	`http://portal.upol.cz`

Declaration of originality

I hereby declare that this thesis is my own work and that, to the best of my knowledge and belief, it contains no material previously published or written by another person nor material which to a substantial extent has been accepted for the award of any other degree or diploma of the university or other institute of higher learning, except where due acknowledgement has been made in the text.

In Olomouc, ..., 2012   ....

Submitted on ...., 2012

The author grants permission to Palacký University in Olomouc to store and display this thesis and its electronic version in university library and on official website.

Acknowledgement

Contents

Chapter 1

Introduction

1.1 Quantum physics

It is the everlasting desire to unravel nature's mysteries that led our 19th century predecessors to carry out a large number of real or *gedenken*[1] experiments. One of the fundamental questions to be answered at that time was the problem of black body radiation. Although several theories existed, none of them was able to fully describe the electromagnetic emissions coming out from a black body [2–4].

It was on December 14, 1900, when a 42 years old German physicist Max Planck proposed an innovative solution to the black body radiation enigma [5]. For the first time he employed the idea of non-continuous transfer of energy between electromagnetic field and matter. His theory, presented that day at the DPG[2] meeting and published year later [6], suggested that energy is exchanged by means of energy packets nowadays called energy quanta. This quantization idea represented a complete revolution in physics leading to explanations of phenomena that classical physics was unable to solve.

From that day on, physicists started to build a completely new theory to explain the nature around us – the quantum theory [7]. The first steps in this path have been laid out by the most important physicist of the beginning of the 20th century like Niels Bohr, Max Born, Louis de Broglie, Paul Adrien Maurice

---

[1]from German, can be translated as "thought", often used to describe imaginary experiments designed to illustrate a theoretical concept on a specific situation (e.g. Schrödinger's cat Gedenkenexperiment [1])

[2]Deutsche Physikalische Gesellschaft, translates as German Physical Society

Dirac, Albert Einstein, Werner Karl Heisenberg, Wolfgang Pauli or Erwin Rudolf Josef Schrödinger and many others. Experiments, like for instance the one by Walther Gerlach and Otto Stern [8], shaped the very fundamental concepts of this theory making it quite different from what physicists were used to. However strange may some of quantum laws seam, there has never been performed any experiment that would contradict the quantum theory and therefore we consider it to be the most advanced theory we have in these days. Even though a century has past from the days quantum physics was born, several fundamental concepts, like for instance the process of quantum measurement, remain clouded by unanswered issues [4].

We do not study nature just because of our desire to understand its laws, but also to gain the capability of using these laws for our benefit. Let us for instance consider classical electronics. Since the first experiments with electromagnetic field [9], scientists sought the ways of how to use it in practical life. It took years of intensive research until the first practical electronic devices were invented [10], but today we can scarcely imagine life without means of modern communications [11]. Similar situation can be observed in the domain of quantum physics. The idea of using quantum laws of nature opens way to a wide range of possible innovations. Quantum metrology for instance offers increased precision of measurements [12–16] that exceeds the capabilities of classical instruments. Also in quantum lithography the improvement of techniques is based on careful usage of quantum laws [17–19]. Another very promising domain of quantum physics based applications is quantum information processing.

1.2   Quantum information processing

Quantum information processing (QIP) is a field of physics and information science trying to employ laws of quantum physics to improve the information processing [20]. The theoretical and experimental research in this domain has already accomplished to provide several important results.

By means of quantum information processing, one can for instance run several practical algorithms faster then it would be possible with classical information processing devices [21]. A famous example of these algorithms is the Shor's algorithm to factorize products of large prime numbers [22, 23]. Using

the so-called quantum Fourier transform, this algorithm is in principle capable of efficient factorisation which can even pose a threat to commonly used classical cryptographic protocols. Several implementations of this algorithm are known [24, 25], but none of them currently provides significant practical applicability.

QIP however allows us to avoid the above mentioned security concerns by offering quantum cryptography [26–32]. This technique makes use of fundamental properties of quantum states and measurements to provide unconditionally secure distribution of information over potentially insecure channel (e.g. eavesdropping on the channel).

It is worth mentioning that also in the field of database algorithms QIP can provide interesting improvement. Groover's algorithm for efficient search in unordered database [33] can be listed as an example.

There are several physical platforms on which QIP schemes can be built including trapped ions, nuclear magnetic resonance, cavity quantum electrodynamics and linear optics. The last one seams particularly suitable for many of the above mentioned applications [34–40]. Namely because light is a very fast and well controllable information carrier. Indeed, many quantum communication protocols and optical QIP circuits are being proposed and experimentally implemented. Three of them, performed by the author, are presented in this thesis.

1.3   Outline

The main contents of this thesis consists of three original QIP experiments with photon pairs (chapters 3 – 5). These experiments were carried out in the Joint Laboratory of Optics of Palacký University and Institute of Physics of Academy of Sciences of the Czech Republic[3]. This workplace has a rich history of quantum information processing research [41, 42]. External co-authors include mainly those from the Department of Optics of Palacký University and then also from Potsdam (Germany) and Poznań (Poland). Although all experiments are dedicated to QIP, they target somewhat different specific areas. For this reason detailed review of relevant research is provided separately at the beginning of each chapter. The text used in chapters 3 – 5 is adopted

---

[3]17. listopadu 50A, 772 07 Olomouc, Czech Republic

from author's journal publications[4] containing the original scientific results. Co-authors' statements confirming Karel Lemr's contribution are attached in the Appendix.

Second chapter of this thesis provides description of employed mathematical formalism. In this chapter, the reader can get familiar with the basic mathematical concepts used to form theoretical framework of later presented experiments. Laboratory equipment such as photon sources, detectors and linear optical components is also discussed in the second chapter to allow better understanding of the experimental setups.

1.3.1 Experiment 1: Preparation of two-photon Knill-Laflamme-Milburn states

Based on *Karel Lemr, Antonín Černoch, Jan Soubusta and Jaromír Fiurášek, Phys. Rev. A* **81***, 012321 (2010)* [A1].

The first experiment presented (chapter 3) addresses the problem of quantum state preparation. In order to function, any QIP protocol requires preparation of particular input quantum state. Input states may also include somewhat complex entangled states that are definitely not trivial to prepare.

This experiment aims on preparing the so-called Knill-Laflamme-Milburn (KLM) states, more precisely their two-photon version. The form of these entangled states was first proposed by Emanuel Knill, Raymond Laflamme and Gerard J. Milburn in their seminal Nature paper discussing efficient quantum computation with linear optics [34]. These authors showed how such a particular class of entangled states can be useful in QIP. Their paper however did not provide any specific recipe for preparation of such states. First general preparation method was derived by Franson *et al.* [43] and subsequently improved by means of tunable controlled phase gates [A2]. A deterministic, experimentally feasible scheme for preparation of two-photon KLM states was first proposed in [A3] and also makes part of author's master's thesis [A4].

Experimental implementation of this proposal is the subject of the third chapter. The experiment was performed in 2009 and published year later [A1].

---

[4]References to author's publications are in the form [An] to distinguish them from other references.

Editors of Nature Photonics included this experiment to Research highlights of the April 2010 issue [44].

1.3.2 Experiment 2: Experimental implementation of the optimal linear-optical controlled phase gate

Based on *Karel Lemr, Antonín Černoch, Jan Soubusta, Konrad Kieling, Jens Eisert and Miloslav Dušek, Phys. Rev. Lett.* **106**, *13602 (2011)* [A5].

The second discussed experiment (chapter 4) is an example of a gate designed for quantum computation. In this particular case the optimal linear optical implementation of tunable controlled phase gate is presented. This two-qubit gate is a quantum analogue to the classical CNOT gate.

Its importance lies in the fact that it belongs to universal set of QIP tools [20]. The theoretical design was derived by our German colleagues Konrad Kieling and Jens Eisert [45]. Subsequent experimental implementation [A5] was performed in 2010 in our laboratory. The gate imposes a tunable phase shift to the state of signal photon, when the control photon is set accordingly. In contrast to previous experimental implementations, the phase shift imposed by our gate can be set to any value in the range between 0 and π. Furthermore, its operation is as much efficient as possible within the framework of linear optics (without additional photon ancillae).

1.3.3 Experiment 3: Experimental linear-optical implementation of a multifunctional optimal cloner

Based on *Karel Lemr, Karol Bartkiewicz, Antonín Černoch, Jan Soubusta and Adam Miranowicz, submitted* [A6].

The third experiment (chapter 5) demonstrates the procedure of quantum cloning. Although it is impossible to perfectly copy an unknown quantum state [46], one can still attempt to do this task approximately [47].

Previous implementations of quantum copying machines optimized their functioning with respect to one specific class of copied states. The implementation presented in the fifth chapter performs symmetric $1 \rightarrow 2$ quantum cloning optimal for various classes of copied states at once [A6]. The versatile

nature of the experimental setup allows incorporating various types of *a priory* information about the cloned state with the goal of maximising fidelity of both output clones.

The theoretical framework was previously discussed in several papers by our Polish colleagues (namely Karol Bartkiewicz and Adam Miranowicz) [48, 49]. Experimental implementation was accomplished in our laboratory by the end of the year 2011 and currently the manuscript is submitted for publication.

During his Ph.D. studies, the author also published several papers not discussed in this thesis. Besides the above mentioned paper on KLM states generation via tunable controlled phase gates [A2], he also published a theoretical paper on generation of atomic Dicke states [A7] and a study on two-photon state analysis [A8]. His popularisation efforts aiming to present experimental QIP to broad audience can be documented on two additional publications [A9, A10].

Chapter 2

Methods and tools

2.1 Quantum description of electromagnetic field

Prior to studying the quantum optical devices, we have to establish suitable description of electromagnetic field. This section presents a simple intuitive method to obtain such description using instruments of quantum theory. Note that more systematic derivation can be found in literature [50, 51], but goes beyond the scope of this thesis. Classical theory [52] gives the energy density of electromagnetic field in free space expressed in the form of

$$H = \frac{1}{2}\left(\epsilon_0|\vec{E}|^2 + \mu_0|\vec{H}|^2\right), \tag{2.1}$$

where $\vec{E}$ and $\vec{H}$ denote the vectors of electric and magnetic intensities. Constants ϵ_0 and μ_0 are called vacuum permittivity and permeability. The Hamilton principle [53] known in classical theoretical mechanics allows to construct equations of motion using the energy expression as a function of generalized coordinates. In the case of electromagnetic field, one can associate these generalized coordinates to the above mentioned electric and magnetic intensities. Such association leads to the analogue between the electromagnetic field on one side and the sum of independent one-dimensional linear oscillators on the other side. Energy of these oscillators expresses in a similar form

$$H = \sum_j \frac{1}{2}\left(P_j^2 + \omega_j^2 X_j^2\right), \tag{2.2}$$

where the generalized coordinates P_j and X_j are the momentum and position of jth oscillator while ω_j represents its angular frequency [54]. In quantum

physics, the concept of linear oscillator is well known and its Hamilton operator (operator of overall energy) takes the form of

$$\hat{H} = \sum_j \frac{1}{2}\left(\hat{P}_j^2 + \omega_j^2 \hat{X}_j^2\right),\tag{2.3}$$

where we have replaced the generalized coordinates by the operators of momentum $\hat{P}_j$ and position $\hat{X}_j$. Inspired by the above mentioned analogue between classical electromagnetic field and classical linear oscillator one can assume that the quantum model for electromagnetic field would also be analogue to the quantum linear oscillator. We therefore define the $\hat{P}_j$ and $\hat{X}_j$ quadrature operators for light and use them to describe the electromagnetic field [7, 55]. Similarly to momentum and position operators the quadrature operators follow commutation relations[1]

$$\begin{aligned}
\left[\hat{X}_j, \hat{P}_k\right] &= i\hbar\delta_{jk}, \\
\left[\hat{X}_j, \hat{X}_k\right] &= \left[\hat{P}_j, \hat{P}_k\right] = 0
\end{aligned}\tag{2.4}$$

with $\hbar$ being the Dirac constant and δ_{jk} the delta function [2]. For the purpose of more convenient calculations, we usually rescale the quadrature operators

$$\hat{x}_j = \sqrt{\frac{\omega_j}{2\hbar}}\hat{X}_j, \quad \hat{p}_j = \sqrt{\frac{1}{2\hbar\omega_j}}\hat{P}_j\tag{2.5}$$

and accordingly also their commutation relations

$$\begin{aligned}
\left[\hat{x}_j, \hat{p}_k\right] &= \frac{i}{2}\delta_{jk}, \\
\left[\hat{x}_j, \hat{x}_k\right] &= \left[\hat{p}_j, \hat{p}_k\right] = 0.
\end{aligned}\tag{2.6}$$

The form of the Hamilton operator composed of the sum of two squares seams similar to the modulus square of a complex number that can also be expressed as a sum of two squares (in this case real and imaginary part). It is therefore convenient to define a new operator

$$\hat{a} = \hat{x}_j - i\hat{p}_j\tag{2.7}$$

called annihilation operator for the reasons soon to be revealed. Its conjugate counterpart is called creation operator and it is defined as

$$\hat{a}^\dagger = \hat{x}_j + i\hat{p}_j.\tag{2.8}$$

---

[1]Commutation is a two-element operation defined as $[a,b] = ab - ba$.
[2]$\delta_{jk} = 1$ for $j = k$, otherwise $\delta_{jk} = 0$

These operators can readily be used to express the Hamilton energy operator

$$\hat{H} = \hbar\omega_j \left(\hat{a}_j^\dagger \hat{a}_j + \frac{1}{2} \right) = \hbar\omega_j \left(\hat{N}_j + \frac{1}{2} \right), \tag{2.9}$$

where number operator $\hat{N}_j = \hat{a}_j^\dagger \hat{a}_j$ is introduced. The term $\frac{1}{2}$ arises from commutation relations and expresses the non-zero energy of the vacuum.

The number operator is important namely because it has the same eigenstates as the Hamiltonian itself. Such states are often called Fock states and follow the eigenvalue equation

$$\hat{N}_j |n_j\rangle = n_j |n_j\rangle, \quad \text{for} \quad n = 0, 1, 2, ...^3 \tag{2.10}$$

The eigenvalues of number operator n_j are non-negative integers and represent the number of photons in the mode in question. Additionally the eigenstates of number operator form an orthonormal basis

$$\langle n_j | m_k \rangle = \delta_{nm} \delta_{jk}, \tag{2.11}$$

which can be used to express other quantum states of light. Note also that the eigenvalue of Hamilton operator corresponding to the eigenstate $|n_j\rangle$ defines the energy stored in such state (in this case $\hbar\omega_j \left(n_j + \frac{1}{2} \right)$).

The role of annihilation and creation operators become apparent, when considering their action on Fock states. It is easy to prove that

$$\begin{aligned} \hat{a}_j |n_j\rangle &= \sqrt{n_j} |(n-1)_j\rangle, \\ \hat{a}_j^\dagger |n_j\rangle &= \sqrt{n_j + 1} |(n+1)_j\rangle, \end{aligned} \tag{2.12}$$

which explains the action of annihilation and creation operators. The annihilation operator decreases the number of photons in a mode by one, whereas the creation operator increases that number by one. Simple algebra reveals the commutation relations for these two operators

$$\begin{aligned} \left[\hat{a}_j, \hat{a}_k^\dagger \right] &= \delta_{jk}, \\ \left[\hat{a}_j, \hat{a}_k \right] &= \left[\hat{a}_j^\dagger, \hat{a}_k^\dagger \right] = 0. \end{aligned} \tag{2.13}$$

---

[3]The $|\bullet\rangle$ is the standard notation for quantum state introduced by P. A. M. Dirac [56].

2.2   Optical qubit

Having the mathematical instruments for quantum optics defined in previous
section, we can now focus on the instruments specific for quantum information
processing. In classical information theory the unit of information is a bit. The
information of one single bit is encoded into an object (information carrier or
memory) using two distinct logical values: 0 and 1. Any classical information
can be represented using a sequence of these logical values. The important fact
is that a bit can be found in either 0 or 1 logical state, nothing else [57].

Quantum physics offers what is known as the superposition principle. This
law states that if there are two possible states in which an object can be found,
the object can also be found in any linear superposition of these states. For
this reason we replace the classical bit by a qubit as the unit of quantum
information [58]. In contrast to classical bit, a qubit can be found in $|0\rangle$ and
$|1\rangle$ basis states or in any of their superposition (e.g. $2|0\rangle - 3|1\rangle$)[4] [20].

It is evident that to physically encode a qubit we need an object that can
support two-level quantum system. Among other physical platforms already
mentioned in the introduction section, photons are very promising. A qubit can
be encoded into the state of photons in several ways. The following discussion
is limited to individual photon encoding often related to the so-called discrete
variables such as the number of photons. Note that also collective multiphoton
states can be used [55, 59], but such instrument is not employed in any of
the presented experiments. This collective multiphoton state encoding is often
related to the so-called continuous variables like for instance light quadratures.

Polarisation encoding belongs to one the most employed especially in bulk
optics (e.g. [60–62]). Figure 2.1 depicts mapping of the qubit state onto the
polarisation degree of freedom. Such mapping is quite straightforward, because
polarisation state "lives" also in a two-dimensional Hilbert space as the qubit
does. So for instance one just associates horizontal polarisation state $|H\rangle$ to
the $|0\rangle$ logical qubit state and vertical polarisation state $|V\rangle$ to the $|1\rangle$ qubit
state. As any superposition of horizontal and vertical polarisation can be
implemented on a single photon, one can use such single photon to carry one
qubit of quantum information.

Besides polarisation, one can also encode the qubit into the spatial degree

---

[4]normalization omitted
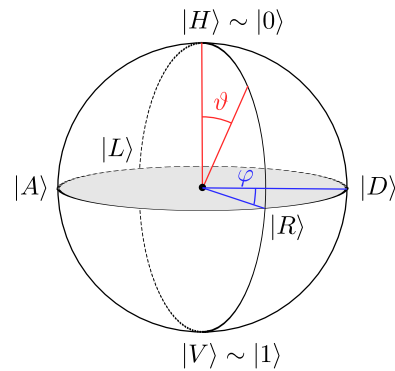
Figure 2.1: Schematic depiction of the Bloch sphere model for polarisation qubit encoding. Horizontal polarisation state $|H\rangle$ is considered $|0\rangle$ logical qubit state while the vertical polarisation state $|V\rangle$ corresponds to logical state $|1\rangle$ of the qubit. Since any linear superposition of the form $[\cos\frac{\vartheta}{2}|H\rangle + e^{i\varphi}\sin\frac{\vartheta}{2}|V\rangle]$ can be implemented on individual photons, polarisation state is a good candidate for qubit encoding. The depiction also includes positions of diagonal ($|D\rangle$) and anti-diagonal ($|A\rangle$) linear polarisation states and right ($|R\rangle$) and left ($|L\rangle$) circular polarisation states for more readability.

Figure 2.2: Illustration of spatial encoding: a) selecting the upper or lower optical mode (fibre) one can encode logical qubit state $|0\rangle$ and $|1\rangle$, b) using a general fibre coupler FC (or beam splitter, see description in section 2.4.1) one can also achieve general superposition of the two encoding paths.

of freedom of individual photons (see figure 2.2). In this case the state of the
photon being in one mode is designated logical $|0\rangle$ state and being in other
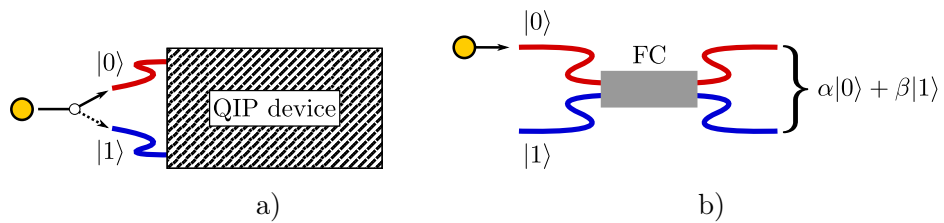mode as $|1\rangle$. Spatial encoding is particularly useful when dealing with fibre-
optical setups (e.g. [63,64]). This is mainly because of the fact that polarisation
state is not maintained while the photon is propagating in a standard fibre.
Note that there exist also polarisation-maintaining fibres, but these are not al-
ways suitable for quantum information experiments namely for their significant
polarisation dispersion.

In some cases the information is encoded both into the polarisation and
spatial degree of freedom. This way, one can transmit more then one qubit of
quantum information using single photon. An example of such mixed encod-
ing is the first presented experiment in this thesis on experimental preparation
of two-photon Knill-Laflamme-Milburn states [A1] or the generation of hyper-
entanglement by Barbieri *et al.* [65].

There are also other degrees of freedom, such as orbital angular momentum
(e.g. [66–68]) or time-bin (e.g. [69, 70]), that can be used for qubit encoding.
Although they offer some advantages and additional space to store quantum
information, they are not used in hereby presented experiments. Note that
spatial encoding also offers to store several qubits within a single photon, but
experimental demands on stability of the whole experimental setup increase
considerably [64].

2.3   Generating photon pairs

Preparation of suitable input photons is an evident prerequisite for experimen-
tal optical quantum information processing. In this section let us now focus
on brief description of the principle of photon sources that have been em-
ployed in later presented experiments. These sources are based on a second or-
der non-linear optical process called spontaneous parametric down-conversion
(SPDC) [71]. As depicted in figure 2.3, Kr^+ continuous wave laser beam of the
wavelength of $413\,nm$ impinges on a non-linear crystal that supports the pro-
cess of SPDC. Either $LiIO_3$ or $\beta\text{-}BaB_2O_4$ (BBO) crystals are used depending
on the experiment.

With a little bit of simplicity the SPDC process is governed by Hamilton
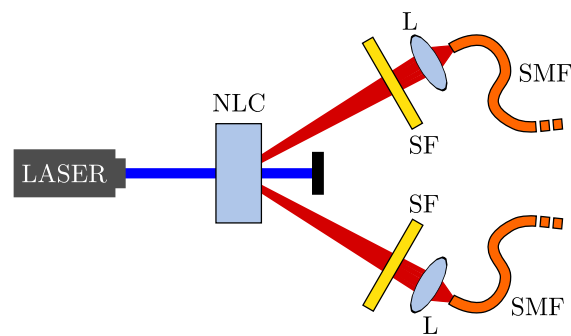
Figure 2.3: Simplified scheme of SPDC based source of photon pairs: pumping laser beam impinges on the non-linear crystal (NLC) inside which some of the pumping photons are converted to pairs of time correlated photons. These photons are coupled to single mode fibres (SMF) using lenses (L). Spectral edge filters (SF) in front of the lenses assure that the diffracted pumping photons do not enter the fibres. Note that realistic experimental setup also consists of a number of translation and rotation stages as well as pinholes to facilitate setup adjustment. To increase the overall efficiency of the source, another lens can be added to focus the pumping beam to the crystal.

operator in the form of

$$\hat{H}_{\mathrm{SPDC}} = \kappa \hat{a}_L \hat{a}_S^\dagger \hat{a}_I^\dagger + \mathrm{h.c.}, \qquad (2.14)$$

where κ represents overall efficiency constant. In the process of SPDC one photon of the laser beam mode L is annihilated yielding a pair of new photons that are created into two different modes called signal S and idler I. Note that due to the spontaneous nature of the process, the exact moment in which one specific photon pair is generated is unpredictable, but once the pair is generated, both photons are created within a narrow time window (typically $100\,\mathrm{fs}$). Detailed evaluation of the SPDC process has to take into account specific characteristics of the used non-linear crystal and the setup geometry. These crystal characteristics and configuration together with energy and momentum conservation laws determine the spectral and spatial geometry of generated photon pairs. These conditions are known in non-linear optics as phase matching conditions. Such a profound discussion is however beyond the scope of this thesis and the reader is encouraged to consult suitable literature [51, 71]. The birefringence of the crystal represents additional degree of freedom defining several types of the SPDC process based on polarisation configuration. Type I was the only used in the hereby presented experiments. In this type, the extraordinary polarised (with respect to crystal's optical axis) pumping photon yields two photons of ordinary polarisation (schematically: $e \to oo$).

For the purposes of majority of QIP experiments, one wishes to obtain completely indistinguishable photons. This requires that the energy of pumping photon is split equally among the created photons. The wavelength of generated photons (in our case $826\,\mathrm{nm}$) then doubles the wavelength of pumping photons. To collect the photons emitted from the crystal, suitable photon couplers have to be used (see figure 2.3). By precise adjustment of their position, one can achieve collection of the individual photons into single mode fibres by means of which the photons are transferred for further processing. Spectral cut-off or interference filters together with single mode fibres assure selection of spectrally and spatially indistinguishable photons.

2.3.1 Generating entangled photon pairs

The above mentioned strategy allows to prepare pairs of time synchronised photons having the same polarisation (for instance horizontal). Their overall
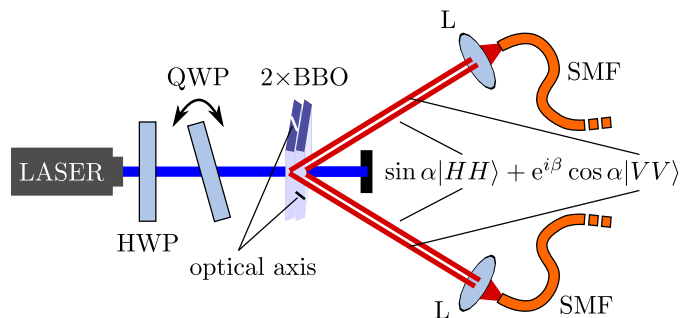
Figure 2.4: Configuration for generating entangled photon pairs using type I SPDC in a pair of BBO crystals: polarisation of the laser beam is modified using half-wave plate (HWP) and quarter-wave plate (QWP), subsequently by means of SPDC it produces coherent superposition of $|HH\rangle$ state of photon pairs in one and $|VV\rangle$ in the other crystal. Due to the indistinguishability of the source crystal and the coherence of the pump beam, the effective generated state is an entangled state of the form of (2.15).

polarisation state is in an ideal case a separable pure state $|HH\rangle$. For many QIP protocols, such an input state would be sufficient, but there are QIP schemes that require entangled photon pairs at their input. One can produce polarisation entangled photons from originally separable state by post-selection [72]. This technique is not suitable in cases where such a post-selection is not compatible with the rest of the setup. Type II SPDC can be used for direct generation of entangled photons [60] without the need for post-selection. However polarisation dispersion and walk-off in type II SPDC has negative impact on the purity of generated entangled states.

In the first presented experiment (chapter 3), an alternative strategy was used. This strategy is based on the proposal by Kwiat *et al.* [73] and it employs two thin (0.6 mm in our case) BBO crystals cut for type I SPDC. These crystals, as depicted in figure 2.4, are rotated so that their optical axis lie in mutually orthogonal planes and then the crystals are optically contacted. One of the crystals therefore converts vertically polarised pumping photons to horizontally polarised photon pairs ($V \to HH$), the other one functions in the opposite way ($H \to VV$). Note that if the crystals are pumped by general elliptic polarisation, both crystals operate simultaneously and the out-

going photons leave the crystals following almost identical paths. Because the pumping polarisation state is pure and because the fibre couplers focused on the crystals' interface can not distinguish in which crystal the photons originate we obtain coherent superposition of $|HH\rangle$ and $|VV\rangle$ which yields an entangled state in the form of

$$|\Psi\rangle_{\text{two photons}} = \sin\alpha|HH\rangle + e^{i\beta}\cos\alpha|VV\rangle. \tag{2.15}$$

In order to control the parameter α, one can rotate a half-wave plate inserted to the pumping beam in front of the crystal. Similarly by tilting a quarter wave-plate in from of the crystal, the parameter β is controlled. This experimentally easy achieved tunability of the generated photon state is one of the most important advantages of this approach. Another advantage of this technique is that there are no problems with polarisation dispersion and walk-off as in the case of type II based sources.

2.4   Linear optical toolbox

The previous sections shed some light on the methods for generating suitable photons and on encoding of quantum information into their states. Now the task is to explain what tools are needed to manipulate the photons and thus process the information stored in their states. To achieve this goal we employ a series of linear optical tools [50, 51, 74] described in this section.

2.4.1   Beam splitter

The most important of all the tools is a beam splitter. Generalising the formalism of this component, one can simply cover the description of other seemingly very different components such as wave plates or filters.

The beam splitter exists under a variety of physical implementations amid which the semitransparent glass plate (see figure 2.5) or fibre coupler are very intensely used. The beam splitter combines two input modes and transforms them into two output modes. Using the annihilation operators defined in (2.7) we can write the transformation equation for input and output modes using the convenient matrix formalism

$$\begin{pmatrix} \hat{a}_{1,\text{out}} \\ \hat{a}_{2,\text{out}} \end{pmatrix} = \begin{pmatrix} \sqrt{T} & \sqrt{R} \\ -\sqrt{R} & \sqrt{T} \end{pmatrix} \begin{pmatrix} \hat{a}_{1,\text{in}} \\ \hat{a}_{2,\text{in}} \end{pmatrix}, \tag{2.16}$$

$$\hat{a}_{1,\text{in}}$$

$$\hat{a}_{2,\text{in}}$$

$$\hat{a}_{2,\text{out}} = \cos\theta\,\hat{a}_{2,\text{in}} - \sin\theta\,\hat{a}_{1,\text{in}}$$

$$\text{BS}(\theta)$$

$$\hat{a}_{1,\text{out}} = \cos\theta\,\hat{a}_{1,\text{in}} + \sin\theta\,\hat{a}_{2,\text{in}}$$
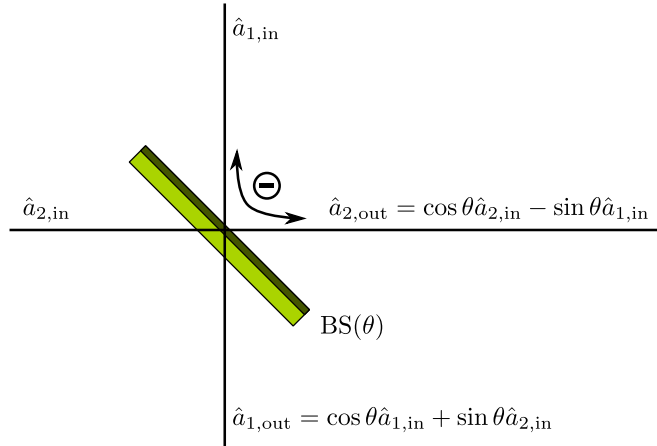
Figure 2.5: Semitransparent glass plate used as a beam splitter: modes 1 and 2 are coherently mixed according to the beam splitter (BS) transformation matrix (2.19). Note that the splitting actually occurs on the plate's surface. One of the reflection changes sign due to boundary conditions. In ideal case, all interfaces other then the splitting interface have 100 % transmissivity.

where T and R stand for intensity transmissivity and reflectivity of the beam splitter. In an ideal case the beam splitter has zero absorbency leading to the energy conservation law expressed as

$$T + R = 1. \tag{2.17}$$

Using this identity we can parametrise the beam splitter by a single parameter θ given by

$$T = \cos^2\theta. \tag{2.18}$$

The transformation equation (2.16) can be rewritten into the form of

$$\begin{pmatrix} \hat{a}_{1,\text{out}} \\ \hat{a}_{2,\text{out}} \end{pmatrix} = \begin{pmatrix} \cos\theta & \sin\theta \\ -\sin\theta & \cos\theta \end{pmatrix} \begin{pmatrix} \hat{a}_{1,\text{in}} \\ \hat{a}_{2,\text{in}} \end{pmatrix}. \tag{2.19}$$

It is evident that the condition for ideal beam splitter (2.17) also ensures that the transformation matrix describes a unitary evolution.

2.4.2 Polarisation dependent beam splitter

Polarisation encoding belongs to one of the most densely used ways to encode quantum information into individual photon states. In order to control this

$$\hat{a}_{1H,\text{in}}$$
$$\hat{a}_{1V,\text{in}}$$

$$\hat{a}_{2H,\text{in}}$$

$$\hat{a}_{2V,\text{in}}$$

$$\hat{a}_{2H,\text{out}} = \cos\theta_H \hat{a}_{2H,\text{in}} - \sin\theta_H \hat{a}_{1H,\text{in}}$$
$$\hat{a}_{2V,\text{out}} = \cos\theta_V \hat{a}_{2V,\text{in}} - \sin\theta_V \hat{a}_{1V,\text{in}}$$

$$\text{PDBS}(\theta_H, \theta_V)$$

$$\hat{a}_{1H,\text{out}} = \cos\theta_H \hat{a}_{1H,\text{in}} + \sin\theta_H \hat{a}_{2H,\text{in}}$$
$$\hat{a}_{1V,\text{out}} = \cos\theta_V \hat{a}_{1V,\text{in}} + \sin\theta_V \hat{a}_{2V,\text{in}}$$
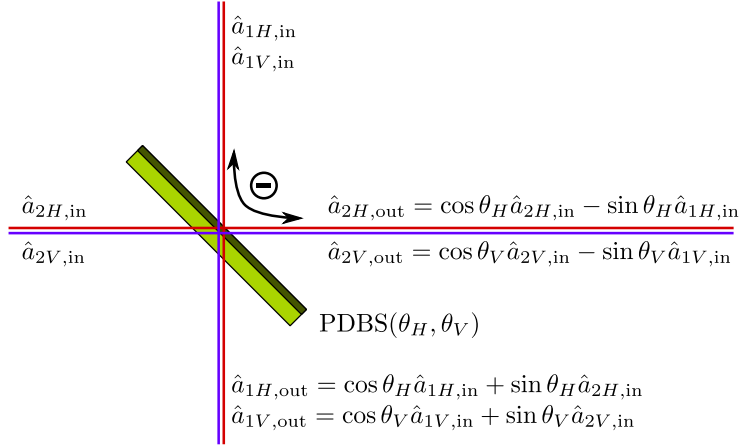
Figure 2.6: Polarisation dependent beam splitter (PDBS): specially designed glass plate with polarisation sensitive reflection coating can be used to function as a beam splitter having different splitting ratios for different polarisations. Note that the orthogonal polarisations (horizontal H and vertical V) do not mix together and the beam splitter thus functions as two separate ordinary beam splitters on one single plate.

degree of freedom in an experiment, polarisation sensitive optical components has to be used. These also include the so called polarisation dependent beam splitter (PDBS) depicted in figure 2.6. To describe such beam splitter, one has to increase the number of both input and output modes to four: two spatial modes for horizontal and two spatial modes vertical polarisation. Generalising the equation (2.19) one can obtain matrix transformation of an ideal polarisation dependent beam splitter in the form of

$$
\begin{pmatrix}
\hat{a}_{1H,\text{out}} \\
\hat{a}_{1V,\text{out}} \\
\hat{a}_{2H,\text{out}} \\
\hat{a}_{2V,\text{out}}
\end{pmatrix}
=
\begin{pmatrix}
\cos\theta_H & 0 & \sin\theta_H & 0 \\
0 & \cos\theta_V & 0 & \sin\theta_V \\
-\sin\theta_H & 0 & \cos\theta_H & 0 \\
0 & -\sin\theta_V & 0 & \cos\theta_V
\end{pmatrix}
\begin{pmatrix}
\hat{a}_{1H,\text{in}} \\
\hat{a}_{1V,\text{in}} \\
\hat{a}_{2H,\text{in}} \\
\hat{a}_{2V,\text{in}}
\end{pmatrix},
$$
(2.20)

where indexes H and V denote horizontal and vertical polarisations. Note that the splitting ratio parameters θ_H and θ_V for H and V polarisations are allowed to be generally different.

Specially designed polarisation dependent beam splitters can be used for

instance in quantum cloning experiments [75]. Another somewhat trivial case of the polarisation dependent beam splitter is the polarising cube – an optical tool for splitting horizontal and vertical polarisations. In this case the horizontal polarisation is completely transmitted while the vertical polarisation is completely reflected ($\theta_H = 0$, $\theta_V = \pi/2$).

2.4.3 Wave plates

To control the polarisation of light within one single spatial mode, one uses the birefringent wave plates. Two prominent cases of these wave plates include the so-called half-wave and quarter-wave plates. The first mentioned is designed to impose a half-wave phase shift between polarisations along its fast and slow optical axis. The later imposes quarter-wave phase shift. These wave plates are sufficient to change the polarisation state of light. It can be shown that any pure polarisation can be changed to any other pure polarisation by a series of a quarter-wave, a half-wave and a second quarter-wave plate.

The beam splitter formalism is also convenient for describing the action of wave plates. Matrix transformation imposed by a half-wave plate reads

$$\begin{pmatrix} \hat{a}_{H,\text{out}} \\ \hat{a}_{V,\text{out}} \end{pmatrix} = \begin{pmatrix} \cos 2\alpha & \sin 2\alpha \\ \sin 2\alpha & -\cos 2\alpha \end{pmatrix} \begin{pmatrix} \hat{a}_{H,\text{in}} \\ \hat{a}_{V,\text{in}} \end{pmatrix} \tag{2.21}$$

with α denoting the angle between plate's fast optical axis and direction of horizontal polarisation.

In a similar way the quarter-wave plate transformation equation can be written in the form of

$$\begin{pmatrix} \hat{a}_{H,\text{out}} \\ \hat{a}_{V,\text{out}} \end{pmatrix} = \frac{1}{\sqrt{2}} \begin{pmatrix} 1 - i\cos 2\alpha & -i\sin 2\alpha \\ -i\sin 2\alpha & 1 + i\cos 2\alpha \end{pmatrix} \begin{pmatrix} \hat{a}_{H,\text{in}} \\ \hat{a}_{V,\text{in}} \end{pmatrix}. \tag{2.22}$$

2.4.4 Phase shift

To complete the list of linear optical tools for QIP with individual photons, let us now focus on the phase shifts. Formally a single mode phase shift is described by the transformation

$$\hat{a}_{\text{out}} = \mathrm{e}^{i\varphi}\hat{a}_{\text{in}}, \tag{2.23}$$

where φ denotes the imposed phase shift. Because the overall phase of a quantum state can be neglected, the phase shift is observable only when comparing

phase difference between two modes (spatial or polarisation). This is very of-
ten the case in interferometric experiments where photons in one arm of the
interferometer are subjected to different phase shift then photons in the other
arm.

Although the mathematical description of the phase shift seams fairly sim-
ple, its experimental implementation may become challenging. In the case of
spatial mode encoding, the phase shift is achieved by means of piezo driven
translation of a mirror or a pentaprism. The stability of such procedure often
requires active stabilisation using either parallel strong optical signal (laser
beam) [76] or, as used in our experiments, repeatedly interrupting the mea-
surement and stabilising on the individual photons themselves [A1, A5].

2.4.5   Neutral density filter

To demonstrate the versatile nature of the beam splitter formalism, let us
now describe the action of a neutral density filter of transmissivity T in an
optical scheme. One would expect the filter to be governed by a single mode
transformation equation

$$\hat{a}_{\mathrm{out}} = \sqrt{T}\hat{a}_{\mathrm{in}}. \tag{2.24}$$

Although this equation is intuitive, it is in violation of the commutation rela-
tions for annihilation and creation operators (2.13). In order to describe the
filter consistently with quantum optics, one has to adopt the notion of ancillary
modes. In this case an ancillary mode is some sort of virtual spatial mode that
is originally in vacuum state and after being coupled to the filtered mode it is
no longer considered in the rest of the experiment. The filter can then be de-
scribed as a beam splitter coupling the filtered mode with the ancillary mode.
Matrix transformation (2.16) is a correct mathematical model for a neutral
density filter supposing the filter intensity transmissivity is T, the first mode is
the filtered mode and the second mode is the above mentioned ancillary mode.
Note that with respect to the description above, a beam splitter can also be
used as a single mode filter.

2.4.6   Beam divider assembly

Sometimes the experiment requires to implement polarisation dependent losses.
This can be achieved by a simple glass plate tilted by suitable angle so that
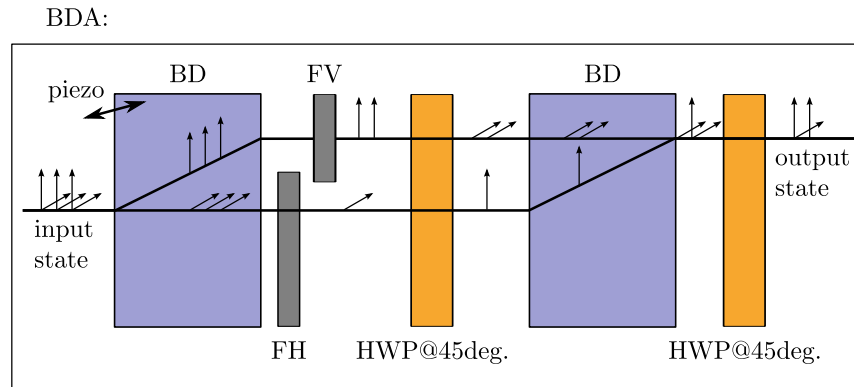
Figure 2.7: Schematic representation of the beam divider assembly (BDA): general input polarisation state containing both horizontal and vertical polarisation enters the first beam divider (BD). There the horizontal polarisation continues following the original path while the vertical polarisation is shifted due to walk-off and leaves the BD 4 mm above propagating in parallel direction. Two gradient neutral density filters are positioned to act on horizontally polarised beam (FH) and vertically polarised beam (FV) separately. To illustrate this effect, hereby depicted filters have different optical densities. Half-wave plate (HWP) rotated at 45 deg. (with respect to horizontal polarisation) follows the filters. Its action swaps horizontal and vertical polarisations allowing them to be recombined on the second BD which operates identically as the first one. To compensate for this swap, second HWP is inserted at the output of the second BD. Additionally mounting one of the BD on a piezo tilt one can also impose tunable phase shift between the polarisation modes.

two orthogonal polarisations have different transmissivities. This approach has however several limitations. Firstly it may affect the beam properties and secondly the achieved losses can not be easily set to any value in the range between 0 and 100 %.

Instead of using the glass plate, in the second and third experiment we employ a compact device called beam divider assembly (BDA). It is worth a brief discussion since it proves to be a very useful tool for polarisation manipulation including an efficient way to achieve polarisation sensitive filtering.

The scheme of this instrument is depicted in figure 2.7. It consists of two beam dividers which separate horizontal and vertical polarisations similarly

as an ordinary polarising beam splitter. The difference lies however in the spatial geometry of output modes. In contrast to the polarising beam splitter, beam dividers outputs both polarisations to two parallel beams separated by a constant distance (in our case 4 mm). In the beam divider assembly, the first beam divider is used to split the two polarisations and the second beam divider to rejoin them. In order to function inversely, the second beam divider has to be preceded by a half-wave plate (set to 45 deg. with respect to horizontal polarisation) which swaps horizontal and vertical polarisations. To cancel such polarisation swap, another half-wave plate (also set to 45 deg.) has to be placed behind the whole assembly. To impose polarisation dependent losses one can position neutral density filters between the two beam dividers so that each of the filters affect only one beam (one polarisation). This proves to be a very efficient and stable way to introduce polarisation sensitive losses. This technique does not burden the experiment by adding any polarisation dispersion and the filtering is tunable in the whole range from zero to unity transmissivity. The stabilisation requires to maintain a constant phase shift between the two split beams. By building the whole beam divider assembly using a compact "cage system"[5], one can achieve very good phase stability of $\lambda/100$ lasting for hours. Setting of the required phase shift can be achieved by usage of a piezo tilt of one of the beam dividers.

2.5   Quantum state analysis

2.5.1   Single photon detection

In order to read the information stored in optical qubits, one has to be able to detect individual photons. There is a variety of detectors that can achieve such sensitivity including iCCD (intensified CCD), EM-CCD (electron multiplying CCD), APD (avalanche photo-diodes), HPD (hybrid photo-detector), photo-multiplier, TES (transition edge sensor) or nanowires [74, 77].

In all of the experiments described in this thesis, APD based single photon counting modules (SPCM) were used as light detectors. Typical quantum efficiency of these detectors is about 60 % which prevents reliable vacuum de-

---

[5]See laboratory equipment manufacturer website for details `http://thorlabs.com/navigation.cfm?Guide_ID=2002`

tection (detection of no photons). APD detectors are also insensitive to the number of impinging photons which limits their usage as photon number resolving detectors. Note that by means of time multiplexing achieved by specially designed fibre loops, these detectors can be used to determine the number of photons in a wave packet [78].

One can construct a formal description of the APD detectors using two-component POVM composed of projection operators on Fock states. The projection operator corresponding to no-detection (no-click) reads

$$\hat{\Pi}_{\text{NO CLICK}} = \sum_{n=0}^{\infty} (1-\eta)^n |n\rangle\langle n|, \tag{2.25}$$

where n stands for the Fock state number and η is the quantum efficiency of the detector. The positive detection event (click) can be regarded as a complementary event to the no-detection

$$\hat{\Pi}_{\text{CLICK}} = \hat{\mathbb{1}} - \hat{\Pi}_{\text{NO CLICK}}. \tag{2.26}$$

In the case of two-photon experiments one needs to distinguish coincidences – simultaneous detection events from two detectors at once. This is achieved by means of coincidence logic – an electronic equipment capable of post-selecting only the cases when two detectors detected photons within specified time interval (in our case 1 ns).

2.5.2 Quantum state tomography

To fully characterize the photon state, one has to perform its tomography. This procedure consists of a series of repeated measurements designed to gather enough data to reconstruct density matrix of the quantum state in question.

In the case of two-photon polarisation encoded quantum states (which is the case for all later presented experiments) the quantum state tomography is achieved by measuring the coincidence rates for different polarisation projections on both photons (see figure 2.8). More specifically all mutual combinations of single photon projections onto horizontal, vertical, diagonal and anti-diagonal linear polarisations and onto right and left circular polarisations are implemented. In every case the corresponding coincidence rate is measured. Subsequently using the method of maximum likelihood, one can estimate the most fitting two-photon density matrix based on the registered coincidence rates [79, 80].
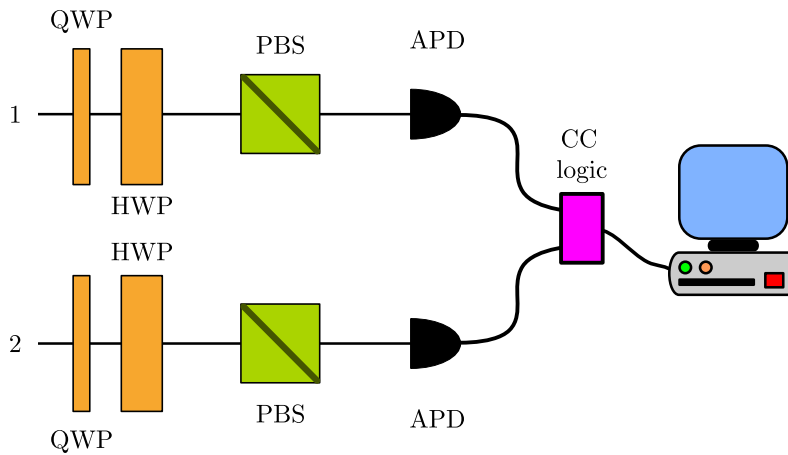
Figure 2.8: Two-photon polarisation tomography setup: photons in arm 1 and 2 gradually propagate through a quarter-wave plate (QWP) and half-wave plate (HWP) mounted on motorised rotation stages. Together with polarising beam splitter (PBS) the wave plates allow projection of individual photons to horizontal, vertical, diagonal and anti-diagonal linear and right and left circular polarisation states. Performing 36 two-photon projections consisting of all combinations of above mentioned single photon projections, one can perform complete state tomography. Avalanche photo-diodes (APD) are used to detect individual photons and coincidence logic (CC logic) then processes the signal to determine the coincidence rates.

2.6   Quantum process tomography

A yet more complex strategy has to be used to fully characterize the whole QIP device. A simple output state tomography is not sufficient because the device generally functions differently for different input states. In this case one has to implement complete process tomography. This procedure consists of setting all combinations of the above mentioned polarisation states as input states and performing output state tomography for every one of them. Similar estimation based on the method of maximum likelihood can determine the Choi matrix isomorphic to the complete positive map describing the action of the device at hand [81–84].

Chapter 3

Preparation of two-photon Knill-Laflamme-Milburn states

Text adopted from *Karel Lemr, Antonín Černoch, Jan Soubusta and Jaromír Fiurášek, Phys. Rev. A* **81**, *012321 (2010)* [A1].

3.1 Introduction

One of the major setbacks of QIP with light is the probabilistic nature of almost all of the QIP schemes. Typically, the success probability decreases with increasing complexity of the scheme. However, as showed by Knill, Laflamme and Milburn this disadvantage may be overcome by employing a specific class of ancillary entangled multiphoton states (referred to as KLM states) that may reduce the failure probability of linear optical quantum gates to arbitrarily small value inversely proportional to the size of the multi-photon KLM state [34]. Besides the capability of increasing success probability of complex quantum computational schemes, the KLM states have been known to enhance other QIP tasks as well. Even the two-photon KLM states can be employed to perform quantum state teleportation and error correction [85].

This chapter describes the first experimental generation and full characterization of the entangled two-photon KLM states. Our experiment follows a recent theoretical proposal by Lemr and Fiurášek [A3], who showed that spontaneous parametric down-conversion (SPDC) along with linear optical components is sufficient to prepare the two-photon KLM states in a more general
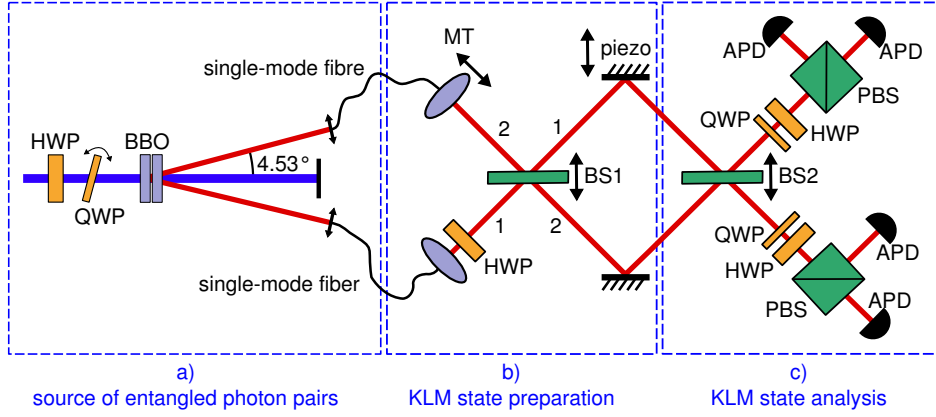
Figure 3.1: Experimental setup for KLM state preparation is divided into three main parts: a) source of entangled photon pairs, b) KLM state preparation and c) KLM state analysis. Optical components are labelled as follows: HWP - half-wave plate, QWP - quarter-wave plate, BBO - non-linear crystals, MT - motorized translation, BS - beam splitter, PBS - polarising beam splitter, APD - set of cut-of filter, single-mode fibre and avalanche photodiode. Spatial modes are labelled 1 and 2 respectively.

form put forward by Franson et al. [86],

$$|\psi_{\mathrm{KLM}}\rangle = \gamma|1100\rangle + \delta|1001\rangle - \gamma|0011\rangle. \tag{3.1}$$

Here γ and δ are real numbers satisfying the normalisation condition $2\gamma^2 + \delta^2 = 1$ and "0" and "1" denote the number of photons in the first through fourth spatial mode. It is easy to see that by means of polarising beam splitters the state (3.1) can be transformed into state of two spatial modes and two polarisation modes,

$$|\psi_{\mathrm{KLM}}\rangle = \gamma|H_1V_1\rangle + \delta|H_1V_2\rangle - \gamma|H_2V_2\rangle, \tag{3.2}$$

where $|H\rangle$ and $|V\rangle$ denote state of a single photon with horizontal and vertical linear polarisation, respectively, and subscripts 1 and 2 label the two spatial modes.

3.2   Experimental setup

Our experimental setup for generation and characterization of the states (3.2) is shown in fig. 3.1. It can be divided into three main parts: source of entangled photon pairs, KLM state preparation and KLM state analysis. To generate an entangled two-photon state, we use a pair of BBO type I ($e \to oo$) non-linear crystals as proposed by Kwiat et al. [73] and introduced in section 2.3.1 (see fig. 3.1a). The optical pumping is supplied by cw Krypton-ion laser at the wavelength of 413.1 nm and about 200 mW of optical power. Before impinging on the crystals, the pumping beam passes through a half-wave plate (HWP) and quarter-wave plate (QWP) so that we can set arbitrary polarisation of the beam. Non-linear processes of SPDC $H \to VV$ and $V \to HH$ are occurring coherently and simultaneously in the first and the second crystal, respectively. Because of the fact that these two processes are indistinguishable, the resulting state of the emitted photon pairs can be expressed as a coherent superposition of two terms,

$$|\Phi_1\rangle = \sin\alpha|H_1 H_2\rangle + \mathrm{e}^{i\phi}\cos\alpha|V_1 V_2\rangle, \qquad (3.3)$$

where subscripts 1 and 2 label the spatial modes. Parameters α and ϕ can be controlled by rotation of HWP and tilt of QWP in the pump beam.

Photons in the state (3.3) are transferred by two single-mode optical fibres to the entrance of the second part of our setup - the KLM state preparation (see fig. 3.1b). The single-mode fibres serve also as spatial mode filters allowing us to reach high interference visibility. First of all, we swap the polarisation of one photon of the pair by putting a diagonally rotated HWP into its path. The resulting state reads,

$$|\Phi_2\rangle = \sin\alpha|V_1 H_2\rangle + \mathrm{e}^{i\phi}\cos\alpha|H_1 V_2\rangle. \qquad (3.4)$$

Subsequently the photons are coherently superposed on the beam splitter BS1. Both beam splitters BS1 and BS2 are attached to a micro-translation stages and can be transversally shifted as depicted by the arrows. Path of the reflected beam depends strongly on the beam splitter positioning, while the transmitted beam is left almost unaffected. By shifting the beam splitter we are thus able to tune its effective reflectivity/transmissivity ratio in the range from 50:50 to 0:100. This operation can be expressed as a linear transformation of the

annihilation operators,

$$\hat{a}_{1,\text{out}} = \frac{1}{\sqrt{2}} \left(\hat{a}_{1,\text{in}} + \sigma \hat{a}_{2,\text{in}} + \sqrt{1-\sigma^2}\, \hat{a}_{1,\text{vac}} \right),$$

$$\hat{a}_{2,\text{out}} = \frac{1}{\sqrt{2}} \left(\hat{a}_{2,\text{in}} - \sigma \hat{a}_{1,\text{in}} + \sqrt{1-\sigma^2}\, \hat{a}_{2,\text{vac}} \right), \tag{3.5}$$

where $\hat{a}_{j,\text{vac}}$ denote annihilation operators of auxiliary vacuum modes. The effective amplitude reflectance $\sigma \in [0,1]$ as defined by (3.5) is set by the position of the beam splitter on the micro-translation and can be adjusted as needed. After the interference on BS1 the state conditioned on presence of both photons in the signal output modes reads,

$$
\begin{aligned}
|\Phi_3\rangle \;=\; & \frac{1}{2} \Big[\sigma \left(\sin\alpha + e^{i\phi}\cos\alpha \right) \left(|H_1 V_1\rangle - |H_2 V_2\rangle \right) \\
& + \left(\sin\alpha - \sigma^2 e^{i\phi}\cos\alpha \right) |V_1 H_2\rangle \\
& + \left(e^{i\phi}\cos\alpha - \sigma^2 \sin\alpha \right) |H_1 V_2\rangle \Big].
\end{aligned} \tag{3.6}
$$

To prepare the KLM state (3.2) one needs to nullify the amplitude of the undesired term $|V_1 H_2\rangle$. This can be achieved by setting $\phi = 0$ and $\sigma = \sqrt{\tan\alpha}$. This choice ensures that the resulting state (3.6) becomes equivalent to the required KLM state (3.2) with real parameters γ and δ satisfying

$$\frac{\gamma}{\delta} = \frac{\sqrt{\sin\alpha\cos\alpha}}{\cos\alpha - \sin\alpha}. \tag{3.7}$$

From this equation we can determine α for any target ratio γ/δ that fully specifies the KLM state (3.2).

We begin the experiment by performing the photon source adjustment. Beam splitters BS1 and BS2 are shifted to the 0:100 position ($\sigma = 0$) during this phase so that we can perform the quantum state tomography and estimation [79] of the state $|\Phi_2\rangle$ generated by the crystals. This tomography determines the values of α and ϕ which can be adjusted by rotation of the HWP and the tilt of the QWP in the pump beam. We have obtained high state purity of about 94-98% and fidelity about 94%. After the adjustment of the photon source is complete, we put the beam splitter BS1 into position so that $\sigma = \sqrt{\tan\alpha}$. Motorized translation MT is then used to balance the lengths of photon trajectories to maximize the visibility of Hong-Ou-Mandel interference (two-photon temporal overlap) [87] on the beam splitter BS1 where the KLM state is created.
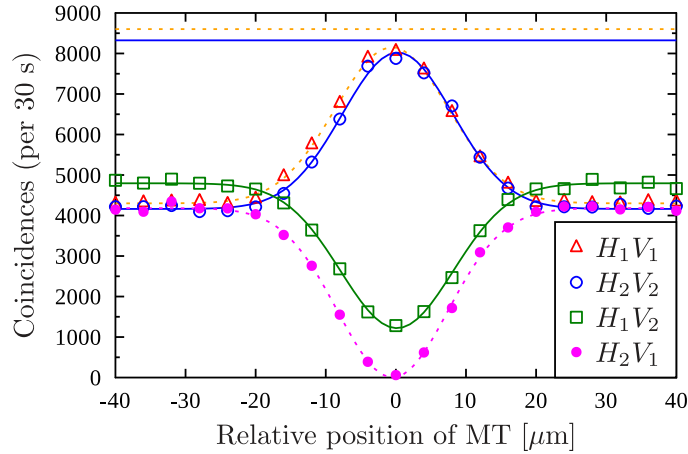
Figure 3.2: Coincidence measurement with the beam splitter BS2 shifted out to 0:100 position. Plotted are the measured coincidences H_1V_1, H_2V_2, H_1V_2 and H_2V_1 (markers) and their respective theoretical Gaussian fits (lines). Relative position of the motorized translation MT has been set so that its origin corresponds to the center of H_2V_1 dip. Error bars are smaller than used marker size.

3.3 State analysis and results

The state analysis is performed in three basic steps using the part "c" of the experimental setup (fig. 3.1c). For the purposes of the first two steps the beam splitter BS2 is tuned to the 0:100 position (it can be considered as effectively removed). The third step of the analysis requires the beam splitter BS2 to be placed into the 50:50 position ($\sigma = 1$).

In the first analysis step we verify that the undesired term $|H_2V_1\rangle$ vanishes due to destructive two-photon interference on BS1. This can be achieved by measuring the coincidences for different positions of the motorized translation (see fig. 3.2). The experimental data clearly shows that the H_2V_1 coincidences realize dip with typical visibility around 95% and they represent only about 0.45% of the sum of all coincidences at the dip. In order to confirm that the prepared state is not contaminated by other unwanted contributions we have further measured the coincidences H_1H_2 and V_1V_2 which turned out to be negligible (less than 150 coincidences per 30 s). Coincidence measurements have also been performed in the diagonal linear polarisation basis. The observed dips in coincidence clicks of two detectors monitoring the same spatial mode

are consistent with the absence of any $|2H, 0V\rangle$ or $|2V, 0H\rangle$ states. These measurements and the high fidelity of the input state with state $|\Phi_2\rangle$, which exhibits perfect anticorrelation of photon polarisations in the H/V basis, permit us to restrict ourselves to a three dimensional Hilbert space spanned by the basis states $|H_1V_1\rangle$, $|H_2V_2\rangle$, $|H_1V_2\rangle$ when characterizing the generated KLM state.

In the second step of our analysis we verify the correct intensity ratios of H_1V_1, H_2V_2 and H_1V_2 terms. We have performed a series of coincidence measurements for different settings of parameter α to demonstrate the correct behaviour of amplitudes γ and δ as functions of α. In fig. 3.3a we plot the experimentally determined ratio of coincidences H_1V_1 and H_2V_2 showing that it approaches well the theoretical value of 1 in all cases. In fig. 3.3b we plot the experimentally determined ratio of coincidences H_1V_1 and H_1V_2 together with the theoretical expectation γ^2/δ^2 given by eq. (3.7). One may observe that the experimentally determined values correspond well to the theoretical prediction.

To fully analyse the prepared KLM state and determine its purity and fidelity one needs to perform a complete state tomography. For this purpose we employ the second beam splitter BS2 and thus form a Mach-Zehnder interferometer. The following three sets of coincidence measurements are carried out: first we measure all coincidences (H_1V_1, H_2V_2, H_1V_2, H_2V_1) with beam splitter BS2 in the 0:100 position (similar measurement as in the previous step). Second we measure the same set of coincidences with BS2 in balanced position 50:50 ($\sigma = 1$) and with zero phase shift between the two arms of the interferometer. Finally we measure with BS2 again in 50:50 position but with relative phase of $\frac{\pi}{4}$ between the two arms. The correct phase can be set using a piezo translation in one of the arms. This measurement requires performing two stabilization procedures: one is the stabilization of the HOM dip on the first beam splitter BS1 and the second is the active stabilization of the phase in the interferometer. Dip stabilization is performed about every $30\,\mathrm{s}$ and MZ interferometer stabilization is carried out about every $5\,\mathrm{s}$.

The three sets of measured coincidences provide sufficient data to fully reconstruct density matrix of the generated KLM states. We have used the well established maximum likelihood estimation method [79] and performed complete state tomography for three different KLM states (see Tab. 3.1). Typical

fidelities of prepared states are about 92% and purities about 90%. As an illustration we present one of the reconstructed density matrices as well as
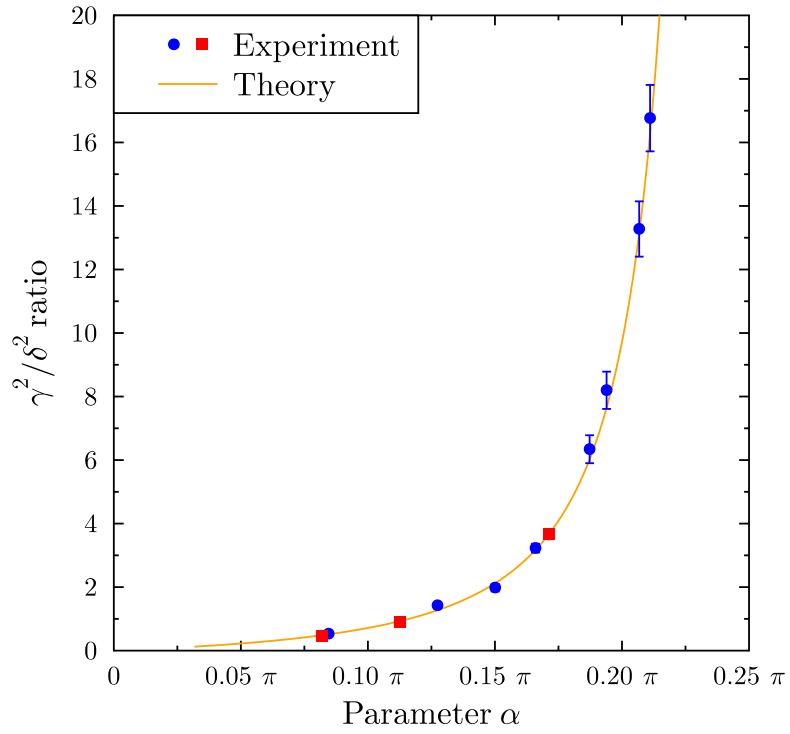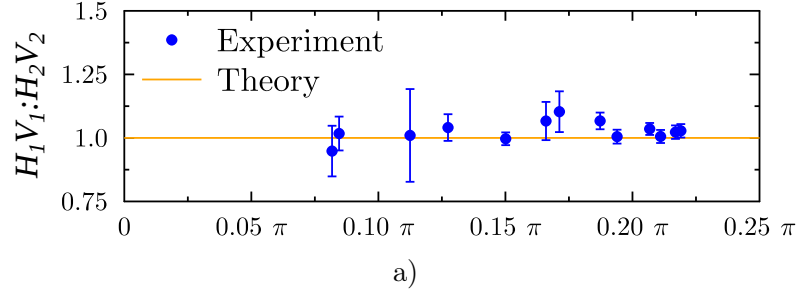

Figure 3.3: a) Ratio of coincidences H_1V_1 and H_2V_2. b) Ratio of coincidences H_1V_1 and H_1V_2. The experimental data with error bars are depicted by blue dots and red squares and the theoretical prediction according to eq. (3.7) is plotted by orange full line.

α	γ^2/δ^2	P	F	F_C
0.17π	3.67	92.4%	93.5%	95.9%
0.11π	0.97	86.0%	91.1%	92.4%
0.08π	0.48	90.4%	92.9%	94.6%

Table 3.1: Purities and fidelities of three prepared KLM states (corresponding to red squares in figure 3.3) with different parameters α. The purity P and fidelity of reconstructed state F is shown together with the fidelity F_C obtained after optimal compensation of local phase shifts.

the related theoretical prediction in fig. 3.4. Non-zero imaginary parts of reconstructed density matrix elements suggest that further improvement of the fidelity F can by achieved by application of local phase shifts, i.e. by transformation $|H_1V_1\rangle \rightarrow |H_1V_1\rangle$, $|H_1V_2\rangle \rightarrow e^{i\theta_1}|H_1V_2\rangle$, $|H_2V_2\rangle \rightarrow e^{i\theta_2}|H_2V_2\rangle$. We have numerically determined the optimal phase shifts θ_1 and θ_2 that maximize the fidelity for given reconstructed density matrix and target KLM state. We present the resulting improved fidelities F_C in the last column of tab. 3.1.

3.4   Conclusions

In summary, we have presented successful experimental preparation of two-photon KLM states using only SPDC photon source and linear optical components. The easy tunability of the entanglement source and of the splitting ratio of the beam splitter allow us to prepare any two-photon KLM state with fidelity about 92% at the expense of losses on the beam splitter BS1 and therefore requiring post-selection of cases when both photons arrive to detectors. These losses can however be overcome by employing a custom unbalanced beam splitter with splitting ratio calculated for some fixed value of α. That way the scheme would not require any post-selection, but it becomes limited to one specific KLM state corresponding to the splitting ratio of the chosen beam splitter.
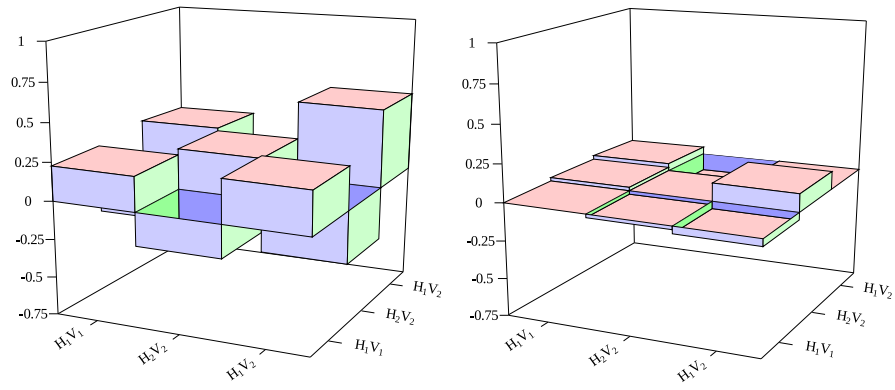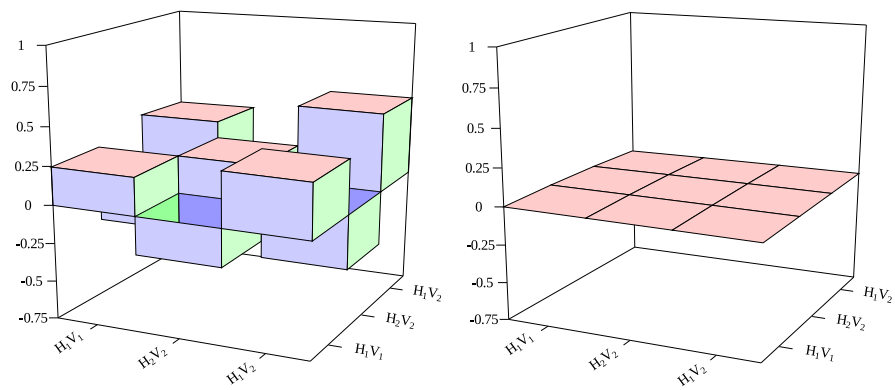
Figure 3.4: a) Real and imaginary parts of reconstructed density matrix of KLM state with $\alpha = 0.08\pi$. b) Theoretically determined density matrix of corresponding pure target KLM state (3.2).

Chapter 4

Experimental implementation of the optimal linear-optical controlled phase gate

Text adopted from *Karel Lemr, Antonín Černoch, Jan Soubusta, Konrad Kieling, Jens Eisert and Miloslav Dušek, Phys. Rev. Lett.* **106**, *13602 (2011)* [A5].

4.1 Introduction

Linear-optical architectures belong to the most prominent platforms for realising protocols of quantum information processing [34–40]. In small-scale applications of quantum information, such as in quantum repeaters, they will quite certainly play a key role. Unsurprisingly, a significant research effort has been dedicated in recent years to experimental realization of universal linear-optical quantum gates. Linear-optical quantum gates are probabilistic by their very nature [34]. Therefore, the exact trade-offs between properties of a gate and its probability of success are in the focus of attention.

In this chapter, we explore such trade-off for the first time experimentally on a controlled-phase gate. We present data from an experimental realization of an optimal linear-optical post-selected controlled phase gate implementing

the following operation on two qubits:

$$
\begin{aligned}
|0,0\rangle &\mapsto u_{0,0}|0,0\rangle = |0,0\rangle, \\
|0,1\rangle &\mapsto u_{0,1}|0,1\rangle = |0,1\rangle, \\
|1,0\rangle &\mapsto u_{1,0}|1,0\rangle = |1,0\rangle, \\
|1,1\rangle &\mapsto u_{1,1}|1,1\rangle = e^{i\varphi}|1,1\rangle,
\end{aligned}
\tag{4.1}
$$

for an arbitrary given phase $\varphi \in [0,\pi]$. It is key to this experiment that this angle can be chosen in a fully tunable fashion, hence adding a flexible scheme to the linear optical QIP toolbox. Post-selected quantum phase gates themselves can be used in order to realize non-demolition measurements, hence rendering post-selected gates truly scalable [88].

Controlled phase gates are important members of the QIP toolbox. For example, they play a key role in the circuit for quantum Fourier transform [20] or quantum simulation tasks [89]. They are entangling quantum gates in general and, together with single-qubit operations, they form sets of universal gates for quantum computing. Notice that the controlled-NOT gate can be obtained by applying a Hadamard transform to the target qubit before and after a controlled phase gate with phase shift π. What is more, non-maximally entangled states can be used in the non-local implementation of controlled phase gates [90–92].

Previous experimental work was devoted to the linear-optical realization of a special case of the controlled phase gate with the fixed phase $\varphi = \pi$ [93–95]. Ref. [96] presents an experiment with phases different from π, but with a non-optimal probability of success. The optimal success probability (without additional photon ancillae) has recently been identified theoretically in ref. [45] and takes the form of

$$
P_C(\varphi) = \left(1 + 2\left|\sin\frac{\varphi}{2}\right| + 2^{3/2}\sin\frac{\pi-\varphi}{4}\left|\sin\frac{\varphi}{2}\right|^{1/2} \right)^{-2}.
\tag{4.2}
$$

This optimum probability we have indeed reached in the described experiment. We observe the quite remarkable trade-off between the phase shift applied by the gate and its success probability, which is — surprisingly — not monotonous in the phase on the interval $[0,\pi]$. The success probability decreases rapidly for small phases, but remains almost constant for phases between $\pi/4$ and π. This experiment is hence expected to be both interesting conceptually as well as technologically.
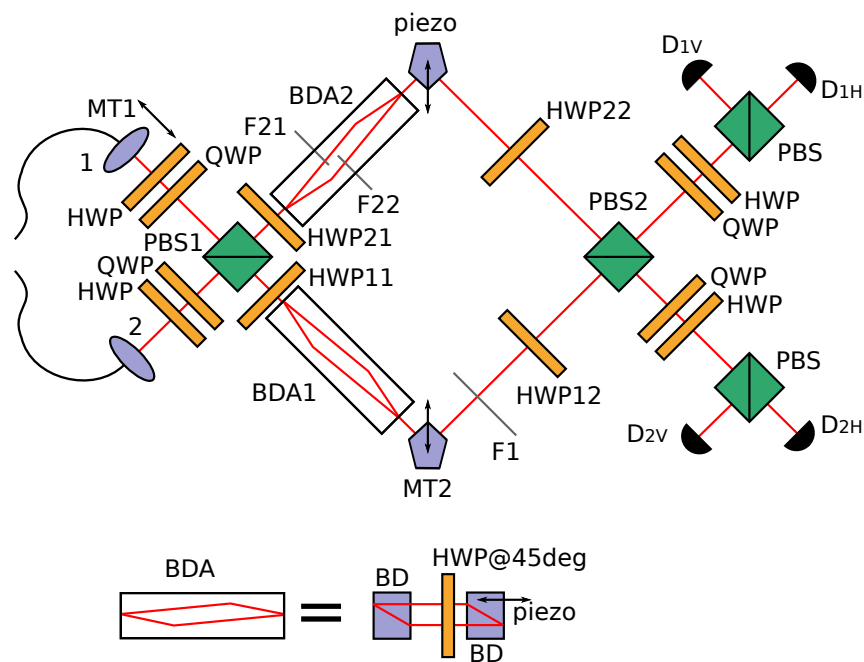
Figure 4.1: Scheme of the experimental setup for implementing a tunable controlled phase gate (see text for details).

4.2 Experimental setup

As the starting point of this experiment, we generate a pair of photons in the process of type I spontaneous parametric down-conversion. The laser beam of $250\,\mathrm{mW}$ of cw optical power emitted by Kr^+ laser at $413\,\mathrm{nm}$ impinges on the $LiIO_3$ crystal. Pairs of photons at $826\,\mathrm{nm}$ are collected using single mode fibres serving also as spatial filters. Subsequently, polarisation controllers are employed to adjust the horizontal polarisation of the photons.

The half-wave plates (HWP) and quarter-wave plates (QWP) in the input arms (see fig. 4.1) are used to set the input states. Subsequently, the photons are superposed on the first polarising beam splitter PBS1 which transmits horizontal and reflects vertical polarisation. Due to imperfections the transmissivity for horizontal polarisation is only $95\,\%$ (the remaining $5\,\%$ are reflected). Polarisation beam splitters also introduce parasitic phase shifts between vertical and horizontal polarisation components. After leaving the PBS1 the photons in the upper arm are subjected to the action of half-wave plate HWP21.

When set to 22.5 deg it performs the transformation $|H\rangle \mapsto (|H\rangle + |V\rangle)/\sqrt{2}$, $|V\rangle \mapsto (|H\rangle - |V\rangle)/\sqrt{2}$, where $|H\rangle$ and $|V\rangle$ denote horizontal and vertical polarisation states, respectively. The lower arm is also equipped with a half wave-plate (HWP11) but it is set to zero (its presence just guarantees the same optical paths, dispersion effects, etc. in the both arms). Behind the wave plates there are the beam-divider assemblies BDA1 and BDA2. They consist of two beam dividers (BD) splitting and subsequently rejoining horizontal and vertical polarisations. BDA2 is equipped with gradient neutral-density filters F21 and F22 (see fig. 4.1). This way one can perform arbitrary polarisation sensitive losses. BDA1 is used just to equilibrate the beam position and the optical length of the both arms. It also avoids potential problems with different dispersion effects in the two arms and makes the setup more flexible. After leaving the beam-divider assemblies the photons propagate through half-wave plates HWP12 and HWP22. HWP22 is set to 22.5 deg reversing thus the transformation imposed by HWP21. HWP12 is set to 45 deg to compensate for the polarisation flip between the H and V polarisations performed by BDA1. The lower arm is equipped with a gradient neutral density filter F1 to apply polarisation independent losses. The gate operation itself is completed by overlapping the photons on the second polarising beam splitter PBS2. To be able to perform complete state and process tomography we employ polarisation analysis in the both output arms. The analysis consists of QWPs and HWPs followed by polarising beam splitters, cut-off filters and single mode fibres leading to single photon detectors. The setup parameters are then adjusted according to theoretical proposal [45] to perform the gate operation (see table 4.1). First we set filters F22 and F1 to introduce the required losses. After that the wave plates HWP21 and HWP22 are set to 22.5 deg. The phase in the beam divider assembly BDA2 is set to maximize the visibility of the interferometer formed by PBS1 and PBS2. The precise tuning of the gate is then performed by switching between the inputs $|H_1, R_2\rangle$ and $|V_1, R_2\rangle$, where indices 1 and 2 denote the input modes and R stands for the right circular polarisation. Using the circular detection basis in the second output arm we can observe the phase applied by the gate when the polarisation of the first input photon flips from $|H\rangle$ to $|V\rangle$. In this configuration we also tune the phase shift inside the beam divider assembly BDA2 and the phase shift between the two arms of the Mach-Zehnder interferometer formed by PBS1 and PBS2.

φ	F1	F22
0	1.00	1.00
0.05π	0.59	0.37
0.125π	0.46	0.27
0.25π	0.37	0.29
0.5π	0.30	0.45
0.75π	0.30	0.69
π	0.33	1.00

Table 4.1: Theoretically calculated intensity transmissivity of neutral density filters F1 and F22 (as depicted in figure 4.1) for seven selected phases φ. The transmissivity of F21 is always 1.

4.3 Results

Gradually we have adjusted the gate to apply 7 phases in the range between 0 and π. Each time we have performed complete process tomography and estimated the process matrix using the maximum likelihood method. Fidelities of the process lie in the range from 84% to 95% (see tab. 4.2). Figs. 4.2 and 4.3 show examples of experimentally obtained process matrices and their theoretical counterparts for $\varphi = \pi$ and $\pi/2$.

For each selected phase we simultaneously measured two-photon coincidence counts between detectors $D_{1H}\&D_{2H}$, $D_{1V}\&D_{2V}$, $D_{1H}\&D_{2V}$, and $D_{1V}\&D_{2H}$, each for 3×3 combinations of polarisation measurement bases in the output arms. This amounts to measuring projections onto horizontal/vertical, diagonal/anti-diagonal and right/left circular polarisations. The diagonal ($|D\rangle$) and anti-diagonal ($|A\rangle$) linear polarisation states are defined as

$$|D\rangle = \frac{1}{\sqrt{2}}(|H\rangle + |V\rangle), \qquad |A\rangle = \frac{1}{\sqrt{2}}(|H\rangle - |V\rangle) \tag{4.3}$$

and the right- ($|R\rangle$) and left-handed ($|L\rangle$) circular polarisation states read

$$|R\rangle = \frac{1}{\sqrt{2}}(|H\rangle + i|V\rangle), \qquad |L\rangle = \frac{1}{\sqrt{2}}(|H\rangle - i|V\rangle). \tag{4.4}$$

The unequal detector efficiencies were compensated by proper re-scaling of the measured coincidence counts [97]. Each measurement was done for 36 different

φ	F_χ	F_{av}	F_{min}	$\mathcal{P}_{\mathrm{av}}$	$\mathcal{P}_{\mathrm{min}}$	$p_{\mathrm{s,obs}}$	$p_{\mathrm{s,th}}$
0	0.939	0.956	0.835	0.960	0.873	0.859±0.013	1.000
0.05π	0.948	0.961	0.906	0.965	0.870	0.366±0.008	0.348
0.125π	0.910	0.903	0.770	0.954	0.866	0.190±0.005	0.210
0.25π	0.842	0.881	0.733	0.896	0.670	0.112±0.003	0.133
0.5π	0.863	0.888	0.815	0.903	0.759	0.090±0.002	0.090
0.75π	0.840	0.868	0.633	0.898	0.705	0.080±0.002	0.088
π	0.835	0.856	0.710	0.922	0.827	0.120±0.001	0.111

Table 4.2: Process fidelities (F_χ), average (F_{av}) and minimal (F_{min}) output-state fidelities, average ($\mathcal{P}_{\mathrm{av}}$) and minimal ($\mathcal{P}_{\mathrm{min}}$) output-state purities and actually observed ($p_{\mathrm{s,obs}}$) and theoretically predicted ($p_{\mathrm{s,th}}$) success probabilities for different phases (φ).

a)   b)
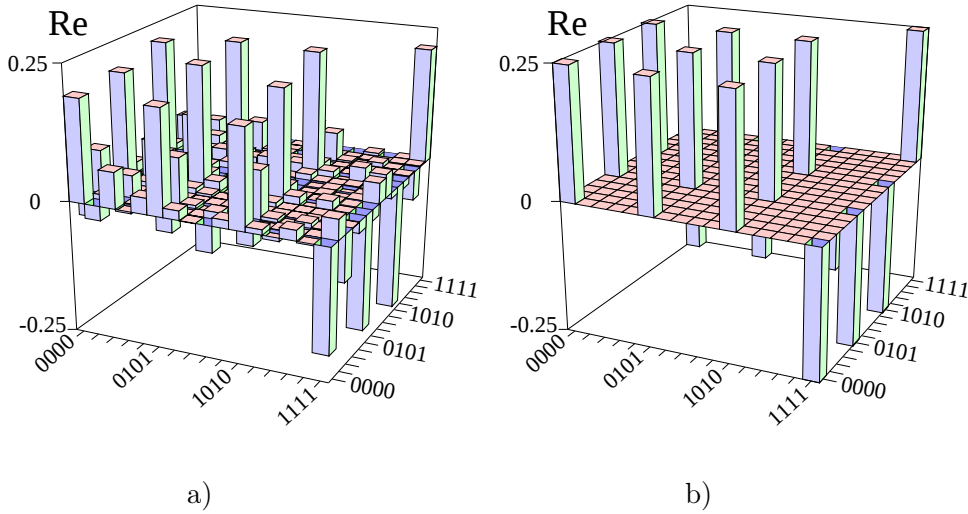
Figure 4.2: Matrix representation of the complete positive map characterizing the operation of the controlled-phase gate with $\varphi = \pi$: a) the left panel shows the real part of the reconstructed process matrix, b) the right one displays the real part of the ideal theoretical CP map. Imaginary parts are small (maximal fluctuations below 0.1). They should be zero in ideal case. The process fidelity $F_\chi = 84\%$.

Figure 4.3: Choi matrices for the gate with $\varphi = \pi/2$: the top panel shows the real (a) and imaginary (b) part of the reconstructed process matrix. The bottom one displays real (c) and imaginary (d) part of ideal matrix. The process fidelity $F_\chi = 86\%$.

input product states. Namely, for 6×6 combinations of polarisation state
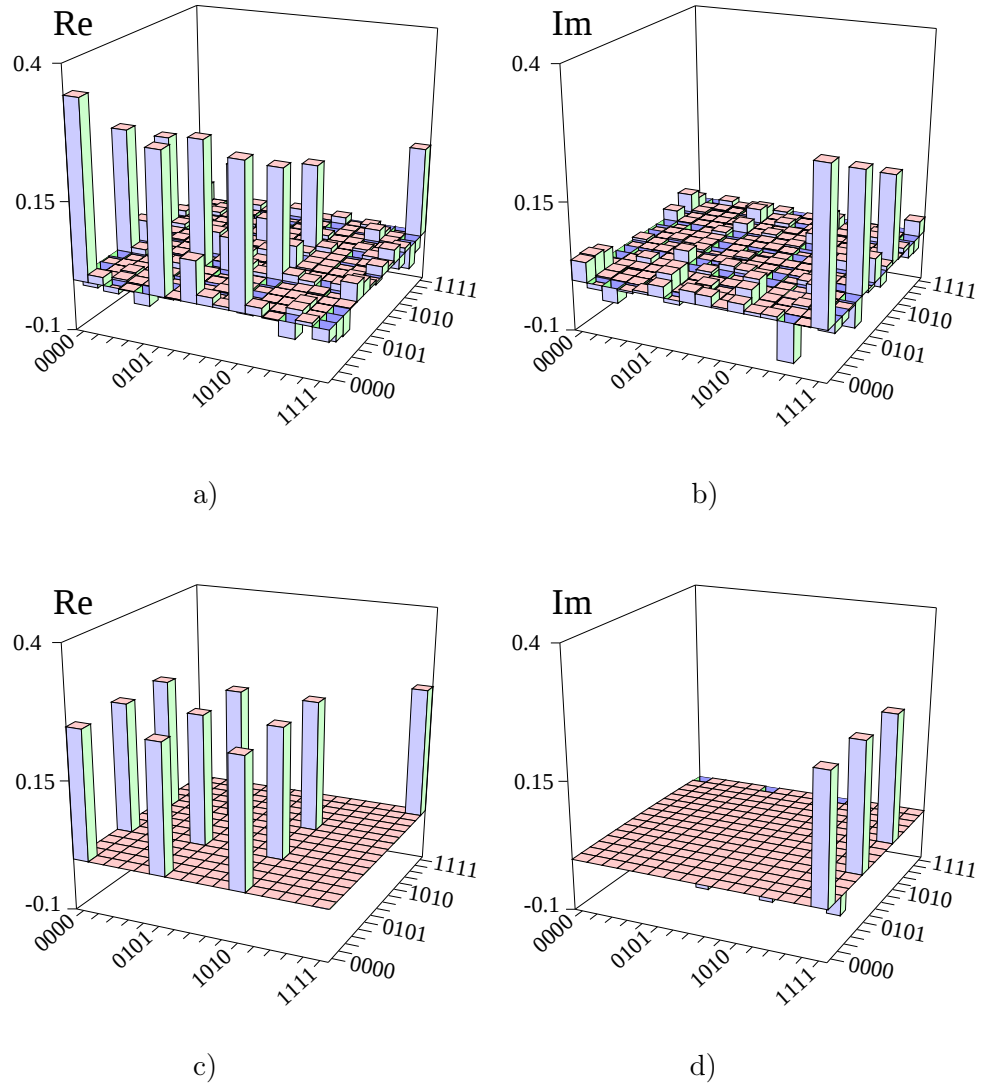vectors $|H\rangle$, $|V\rangle$, $|D\rangle$, $|A\rangle$, $|R\rangle$, and $|L\rangle$ of each input photon. This complex
measurement provided us with tomographically complete data enabling us to
fully characterize the implemented operation by quantum process tomography
[79,83,84,98,99] as well as to reconstruct density matrices of output states for
each used input state.

Each setting of an input and output polarisation basis was preceded by an
active stabilization. For the purpose of the stabilization the fixed input state
and output detection basis were always used. In this setting the visibility in
the interferometer formed by PBS1 and PBS2 was measured. If this visibility
was lower than a selected threshold (usually 94%) then the positions of MT1
(two-photon temporal overlap) and MT2 (equilibration of interferometer arms)
were optimized and the phase drift was compensated. Finally the required
polarisations were set and data were accumulated within 5 s.

Any quantum operation can be fully described by a completely positive
map and — according to the Jamiolkowski-Choi isomorphism — represented
by a positive-semidefinite operator χ on the tensor product of input and output
Hilbert spaces [81,82]. In our case χ is a (16×16) square matrix. From the
measured data we can reconstruct χ for any setting of φ using maximum likeli-
hood estimation [79,80]. To quantify the quality of the operation we calculate
the process fidelity $F_\chi = \mathrm{Tr}[\chi\chi_{\mathrm{id}}]/(\mathrm{Tr}[\chi]\mathrm{Tr}[\chi_{\mathrm{id}}])$. Here χ_{id} represents the ideal
transformation corresponding to the controlled-phase gate. Specifically,

$$\chi_{\mathrm{id}} = \sum_{i,j,k,l=V,H} |i,j\rangle\langle k,l| \otimes U|i,j\rangle\langle k,l|U^\dagger, \qquad (4.5)$$

where U stands for the unitary operator on two qubits defined by eq. (4.1).
We have also reconstructed the density matrices of output two-photon states
corresponding to all product input states $|j,k\rangle$, $j,k \in \{H,V,D,A,R,L\}$. This
was done for seven values of φ. An important parameter characterizing the gate
performance is the fidelity of output states ρ_{out} defined as $F = \langle\psi_{\mathrm{out}}|\rho_{\mathrm{out}}|\psi_{\mathrm{out}}\rangle$,
where $|\psi_{\mathrm{out}}\rangle = U|\psi_{\mathrm{in}}\rangle$ and $|\psi_{\mathrm{in}}\rangle$ is the input state vector. Table 4.2 contains
the average and minimal values of state fidelities for different phases. Fidelities
F_{av} are averaged over all output states corresponding to our 36 input states;
F_{min} denote minimal values. Another important characteristics is the purity
of the output state ρ_{out}, defined as $\mathcal{P} = \mathrm{Tr}[\rho_{\mathrm{out}}^2]$. If the input state is pure the
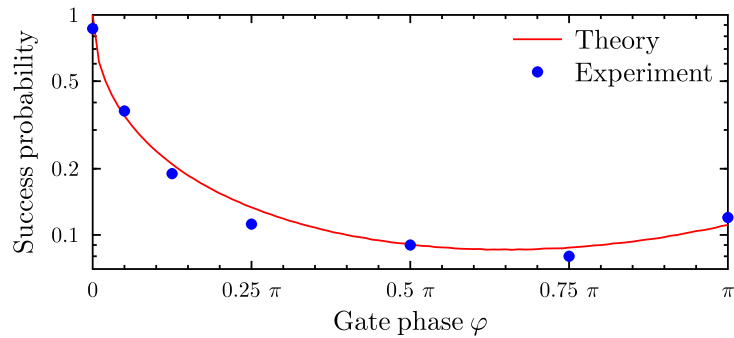
Figure 4.4: Success probability of the controlled phase gate. Circles denote experimental results, full line shows the theoretical prediction.

output state is expected to be pure as well. The average and minimal purities of output states are also given in table 4.2.

4.3.1 Trade off in success probabilities

The most important result of this experiment — aside from the technological implications — is the experimental verification of the trade-off between the phase shift applied by the gate and the corresponding success probability of the gate. We have estimated the success probability for each value of the selected phase shifts. It was calculated as a ratio of the number of successful gate operations per time interval and the number of reference counts during the same interval (measured with no filters and with the wave plates set to 0). We have determined the success probability for all the selected input states. These probabilities were averaged and the standard deviations of the means were calculated. Notice that the calibration measurements collect coincidence counts behind the setup (using the same detectors as in the subsequent measurements), thus all the "technological" losses in the setup (about 60%) and low detector efficiencies are included in the calibration. Therefore the estimated success probabilities are not burdened by these "technological" losses. They can be compared with the theoretical predictions in tab. 4.2 and in fig. 4.4. One can see a very good agreement with the theoretical prediction.

4.4   Conclusions

We have built the first implementation of the tunable linear-optical controlled phase gate which is optimal for any value of the phase shift. Changing the parameters of the setup the gate can apply any phase shift from the interval $[0, \pi]$ on the controlled qubit. We have thoroughly tested the performance of the gate using full quantum process tomography. Obtained process fidelities range from 84% to 95%. We have determined that the main limiting factors for the fidelities are imperfect two-photon spatial and temporal overlap and birefringence of PBS causing partial distinguishability between different polarisation modes. We have also experimentally verified that all our controlled phase gates are optimal in the sense that they operate at the maximum possible success probabilities that are achievable by linear-optical setups. The experimental verification of this trade-off between the phase shift applied by the gate and the corresponding success probability of the gate is the most notable result of our work. It demonstrates the contra-intuitive fact that the optimal success probability is not monotonous with the phase shift increasing from 0 to π. It is the hope that the flexible tool established here proves useful in devising further linear optical circuits for quantum information processing and that ideas developed in this work find their way to realization in fully integrated optical architectures.

Chapter 5

Experimental linear-optical implementation of a multifunctional optimal cloner

Text adopted from *Karel Lemr, Karol Bartkiewicz, Antonín Černoch, Jan Soubusta and Adam Miranowicz, submitted* [A6]

5.1 Introduction

Quantum cloning is one of the most intriguing topics in quantum physics. It is important not only because of its fundamental nature, but also because of its immediate applications to quantum communications including quantum cryptography. Similarly to other important quantum information processing protocols, quantum cloning has witnessed a considerable development over the past two decades. Although it is impossible to perfectly copy an unknown quantum state [46], one can still attempt to do this task approximately. The first design of an optimal cloning machine was suggested by Bužek and Hillery [47]. The cloner is called optimal when it gives the best results allowed by quantum mechanics. Moreover the *universal cloning* (UC) should operate equally well for all possible qubit states [100–104]. In contrast, limiting cloning to a specific subset of qubit states, one can achieve a more precise cloning operation. A prominent example of this situation is the *phase-covariant cloning* (PCC), where only qubit states with equal superposition of $|0\rangle$ and $|1\rangle$ are

considered [75, 105–110].

This chapter addresses a question interesting from both conceptual and practical points of view: how well can quantum state be cloned if some *a priori* information about the state is known. Theoretical investigation of this issue led to quantifying the information known about the cloned state in terms of axially-symmetric distributions on the Bloch sphere [49]. This class of distributions contains an important subclass of distributions which are mirror-symmetric with respect to the equatorial plane. It is therefore convenient to define the *mirror phase-covariant cloning* (MPCC) as a strategy for cloning states with this kind of *a priori* information [48].

We hereby present the first implementation of the MPCC and we also demonstrate that the same setup can be used for optimal cloning in other prominent regimes such as universal cloning and phase-covariant cloning. To our best knowledge, this makes our scheme the first multifunctional cloner ever presented. The device discussed in this chapter represents a symmetric $1 \to 2$ quantum cloner.

5.2   Mirror phase-covariant cloning

In our experiment we cloned the polarisation state of a single photon given by

$$|\psi\rangle = \cos\frac{\theta}{2}|H\rangle + \sin\frac{\theta}{2}\mathrm{e}^{i\varphi}|V\rangle, \qquad (5.1)$$

where $|H\rangle$ and $|V\rangle$ stands for horizontal and vertical polarisation state, respectively. In accord with the original definition [48], we assume $\cos^2\theta_{\mathrm{eff}} = \langle\hat{\sigma}_z\rangle^2$ being the only *a priori* information known about the cloned state, where $\hat{\sigma}_z$ denotes the third Pauli operator. It has been recently demonstrated [49] that the MPCC can also be applied to a wider class of qubit distributions $g(\theta, \varphi)$. Consequently, the optimal cloner for a set of qubits given by a distribution $g(\theta, \varphi)$ is an MPCC set for an axial angle θ_{eff} defined as $\langle\cos^2\theta\rangle = \cos^2\theta_{\mathrm{eff}}$, where the angle bracket stands for averaging over the distribution. Moreover, we note that the mirror-symmetry condition can be weakened and the MPCC transformation can be used as an optimal cloning transformation for other sets of qubits which are not axially-symmetric and do not exhibit the

mirror-symmetry, but rather fulfil the following conditions:

$$\int_0^{2\pi} [g(\theta, \varphi) + g(\pi - \theta, \varphi)] e^{i\varphi n} \mathrm{d}\varphi = 0,$$
$$\int_0^{2\pi} g(\theta, \varphi) \mathrm{d}\varphi = \int_0^{2\pi} g(\pi - \theta, \varphi) \mathrm{d}\varphi, \tag{5.2}$$

where g is a distribution of qubits on the Bloch sphere and $n = 1, 2$. Therefore, any MPCC optimal for some θ_{eff} is also optimal for a wider class of distributions which need to be neither axially-symmetric nor mirror-symmetric but fulfil Eqs. (5.2). The above-mentioned arguments considerably broaden the usefulness of the presented device.

5.3 Experimental setup

The experimental setup (as depicted in fig. 5.1) consists of a special unbalanced polarisation-dependent beam splitter (PDBS) and two beam divider assemblies (BDA1 and BDA2) placed in each of the output modes of the beam splitter. The PDBS employed in this scheme has different transmittances for horizontal (μ) and vertical (ν) polarisations. The transmittances should be given by

$$\mu = \frac{1}{2}\left(1 + \frac{1}{\sqrt{3}}\right), \quad \nu = \frac{1}{2}\left(1 - \frac{1}{\sqrt{3}}\right). \tag{5.3}$$

Due to manufacturing imperfections the observed transmittances of our PDBS are $\mu = 0.76$ and $\nu = 0.18$. Please note that this imperfection can be corrected without the loss of fidelity through suitable filtering at the expense of a lower success rate.

Beam divider assembly is depicted in more detail in fig. 5.1b. It is composed of two beam dividers (BDa and BDb) used to separate and subsequently combine horizontal and vertical polarisations. A neutral density filter (F) with tunable transmittance τ is positioned between the two beam dividers so that one of the paths (polarisations) is attenuated while the other remains intact. Also a half-wave plate (HWPb) is placed between the beam dividers swapping the polarisations and thus allowing them to be recombined at the output of the second beam divider (BDb). To control attenuation of each polarisation by the neutral density filter, we envelope the beam divider assembly by two half-wave plates (HWPa and HWPc). Beam divider assembly is equivalent

a)

b)

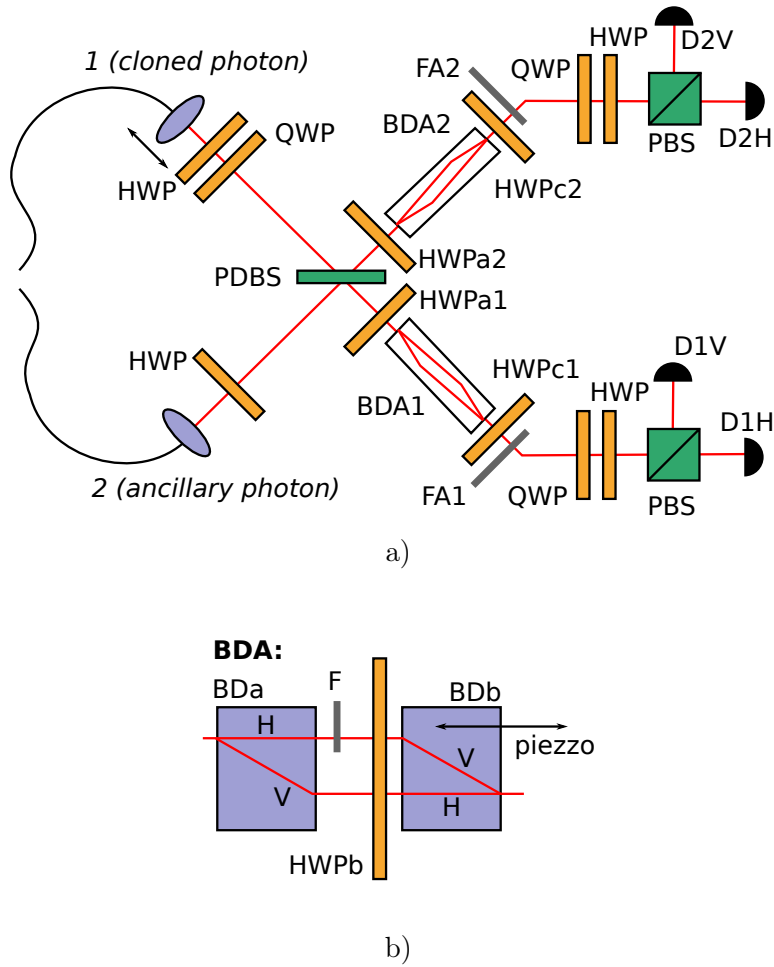Figure 5.1:   a) Scheme of the experimental setup for cloning as described in the text. b) Detailed scheme of the beam divider assembly. Components as labelled as follows: HWP - half-wave plate, QWP - quarter wave-plate, PDBS - polarisation dependent beam splitter, BDA - beam divider assembly, F - neutral density filter, PBS - polarising beam splitter, D - single photon detector, BD - beam divider.

to a Mach-Zehnder interferometer and, by the means of a piezo-driven tilt of one of the beam dividers, we can set an arbitrary phase shift between the two paths (polarisations).

In the ideal case, having $\mu + \nu = 1$, the setup operates as follows. A separable two-photon state $|H_1 H_2\rangle$ (indices denote the mode number) is generated in the process of the type I spontaneous parametric down-conversion using a LiIO$_3$ crystal pumped by cw Kr$^+$ laser at 413 nm of 150 mW optical power. These photons are brought to the input of the setup via single-mode fibres. The parameters to be set for the PCC and UC regimes are just specific cases of the MPCC setting as discussed later. For this reason we now concentrate on the MPCC setting. The polarisation of the first (cloned) photon is set in such a way that it belongs to one of the parallels of latitude on the Bloch sphere with a given polar angle θ (see eq. (5.1)). The second (ancillary) photon remains either horizontally polarised or is randomly swapped in 50 % of the cases to vertical polarisation. After this preparation stage the two photons are coherently overlapped at the PDBS. Depending on the polarisation of the ancillary photon, we perform subsequent transformation. If the ancillary photon remains horizontally polarised we set the half-wave plates (HWPa1 and HWPa2) in front of the beam dividers to 45 deg. so that the vertical polarisation is attenuated in both beam divider assemblies. The level of transmittance τ of the filters F is set according to the relation

$$\tau = \frac{\left(1 - \Lambda^2\right)\left(1 - 2\mu\right)^2}{2\mu\nu\Lambda^2}, \qquad \text{where} \qquad \Lambda = \sqrt{\frac{1}{2} + \frac{\cos^2\theta}{2\sqrt{P}}}, \qquad (5.4)$$

and $P = 2 - 4\cos^2\theta + 3\cos^4\theta$. Additionally we also set a phase shift π between horizontal and vertical polarisation in both output modes. In the case of the ancillary photon being vertically polarised we set the half-wave plates HWPa1 and HWPa2 to 0 deg. and this time subject the horizontal polarisation to the same filtering as given by eq. (5.4). Also we set the phase shift between the polarisations to zero and rotate the half-wave plates HWPc1 and HWPc2 to 45 deg., thus cancelling the polarisation swap exercised by the half-wave plates HWPb1 and HWPb2 (inside the beam divider assemblies).

Finally, the two-photon state polarisation analysis is carried out by measuring the rate of two-photon coincidences for all combinations of single-photon projections to horizontal, vertical, diagonal, anti-diagonal linear, and right and

left circular polarisation. We can then estimate the two-photon density matrix using a standard maximum likelihood method [79].

In order to use the setup in the PCC regime for any latitude angle θ, one just needs to set all the parameters as if performing the MPCC set for the latitude angle $\theta = \pi/2$. In case of the PCC there is no need to randomly swap the horizontal and vertical ancillae. In this case we know the hemisphere to which the cloned states belong so we can simply use the closer ancilla (horizontal for northern and vertical for southern hemispheres).

Similar analysis can be carried out to determine, that the setup actually performs the UC if set to the same parameters as for the MPCC with the polar angle $\theta = \mathrm{acos}(\sqrt{3}/3) \approx 0.304\pi$. In this regime a random swap between horizontal and vertical ancillae is also required.

5.4   Compensating for imperfect transmittances

In our case the equation relating beam-splitter transmittances ($\mu + \nu = 1$) does not hold and we have $\mu + \nu \neq 1$. Hence additional filtering operations are required in order to maintain the maximum achievable fidelity of the setup. This additional filtering manifests itself in two ways. First, one needs to un-balance the ancilla-dependent filtering performed by filters F in both BDAs. We require $\tau_1 = \tau$ and $\tau_2 = \omega\tau$ for the BDA1 and BDA2, respectively, where

$$\omega = \frac{\tau_2}{\tau_1} = \frac{\mu\nu}{(1-\mu)(1-\nu)}. \tag{5.5}$$

Note that $\omega = 1$ in the ideal case for $\mu + \nu = 1$ and $\omega = 0.695$ for the applied PDBS. Second, the realisation of the MPCC with the PDBS where $\mu + \nu \neq 1$ requires applying an additional unconditional filtering. This filtering is polarisation-dependent and is performed regardless of the state of the ancillary photon. The polarisation dependent transmittances τ_H and τ_V for the H and V-polarised photons, respectively, need to satisfy the following relation:

$$\kappa = \frac{\tau_V}{\tau_H} = \frac{2\mu - 1}{1 - 2\nu}, \tag{5.6}$$

where κ is a constant value fixed by the parameters of the PDBS, and both τ_H and τ_V should have the largest possible values in order to maximize the effi-ciency of the setup. Note that in an ideal case, when $\mu + \nu = 1$ is fulfilled, $\kappa = 1$. In our case, we get $\kappa = 0.813$. Therefore, we apply an additional unconditional
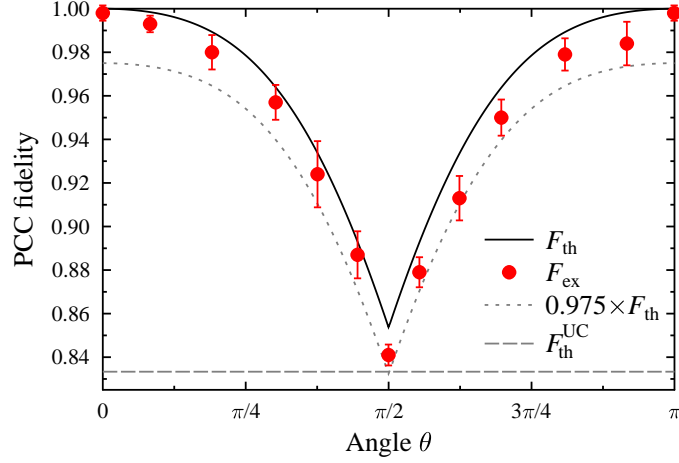
Figure 5.2: Experimental fidelity F_{ex} for the PCC regime depicted against theoretical prediction F_{th} (solid curve). The short-dashed curve indicates the fidelity drop to 97.5% with respect to the corresponding theoretical value. The theoretical fidelity $F_{\text{th}}^{\text{UC}}$ for the UC is also depicted (long-dashed curve).

filtering only for the V-polarised photons since the optimal transmittances are $\tau_V = \kappa$ and $\tau_H = 1$. Please note that for our PDBS $\kappa < 1$, but in the opposite case the best choice of the parameters would be $\tau_V = 1$ and $\tau_H = 1/\kappa$. Moreover, if there are any other systematic uniform polarisation-dependent losses τ'_H and τ'_V we can compensate for them by setting $\kappa = \tau'_H/\tau'_V \times (2\mu - 1)/(1 - 2\nu)$.

To summarise the above-mentioned corrections, the overall filtering operations in the first mode are described by

$$\tau_{1,H} = \tau^{\delta_{V,s}} \text{ and } \tau_{1,V} = \kappa\tau^{\delta_{H,s}}, \tag{5.7}$$

and in the second mode by

$$\tau_{2,H} = (\omega\tau)^{\delta_{V,s}} \text{ and } \tau_{2,V} = \kappa(\omega\tau)^{\delta_{H,s}}, \tag{5.8}$$

where $\delta_{V,s}$ ($\delta_{H,s}$) is Kronecker's delta and is equal to 1 iff the polarisation s of the ancillary photon is V (H).

Angle θ	F_{ex} [%]	F_{th} [%]
0	99.8 ± 0.4	100.0
$\pi/12$	99.3 ± 0.4	99.8
$\pi/5$	98.0 ± 0.8	98.8
$\pi/3$	95.7 ± 0.8	95.3
$3\pi/8$	92.4 ± 1.5	93.4
$\pi/2.25$	88.7 ± 1.1	89.4
$\pi/2$	84.1 ± 0.5	85.4
$\pi/1.8$	87.9 ± 0.7	89.4
$5\pi/8$	91.3 ± 1.0	93.4
$2\pi/3$	95.0 ± 0.8	95.3
$4\pi/5$	97.9 ± 0.7	98.8
$11\pi/12$	98.4 ± 1.0	99.8
π	99.8 ± 0.4	100.0

Table 5.1: Summarised data for the PCC regime. F_{ex} denotes experimentally estimated average fidelity for a given polar angle θ on the Bloch sphere and F_{th} is the theoretical prediction. Note that the error estimated as RMS is just indicative of the actual error, because it does not take into account the physical properties of fidelity.
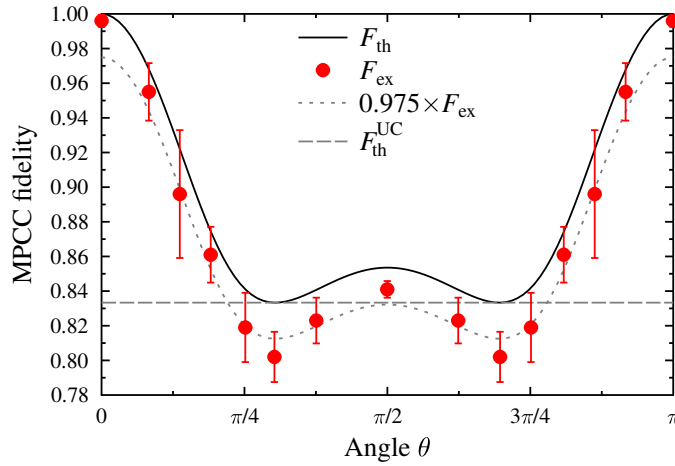

Figure 5.3: Same as in fig. 5.3 but for the MPCC.

Angle θ	F_{ex} [%]	F_{th} [%]	P_{ex} [%]	P_{th} [%]
0	99.6 ± 0.4	100.0	10.5 ± 2.8	10.5
$\pi/12$	95.6 ± 1.7	97.0	10.6 ± 1.9	10.5
$\pi/5$	86.1 ± 1.6	87.4	09.6 ± 0.9	12.1
$\pi/4$	81.9 ± 2.0	84.1	14.0 ± 2.9	14.4
$\pi/3$	80.2 ± 1.5	83.3	19.5 ± 3.5	19.6
$3\pi/8$	82.3 ± 1.3	84.0	23.7 ± 1.5	21.9
$\pi/2$	84.1 ± 0.5	85.4	24.8 ± 0.1	25.0
$5\pi/8$	82.3 ± 1.3	84.0	23.7 ± 1.5	21.9
$2\pi/3$	80.2 ± 1.5	83.3	19.5 ± 3.5	19.6
$3\pi/4$	81.9 ± 2.0	84.1	14.0 ± 2.9	14.4
$4\pi/5$	86.1 ± 1.6	87.4	09.6 ± 0.9	12.1
$11\pi/12$	95.6 ± 1.7	97.0	10.6 ± 1.9	10.5
π	99.6 ± 0.4	100.0	10.5 ± 2.8	10.5

Table 5.2: Same as in Table 5.1 but for the MPCC regime. Moreover P_{ex} and P_{th} denote experimental and theoretical success probabilities.
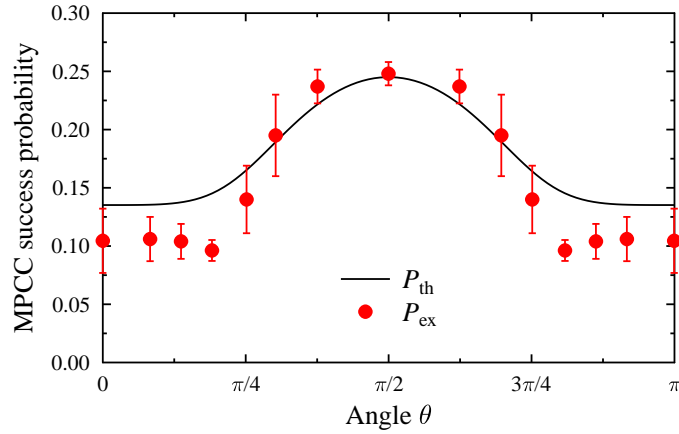

Figure 5.4: The success probability of the MPCC as a function of polar angle θ is depicted: P_{ex} denotes experimentally determined value and P_{th} denotes our theoretical prediction. Note that sometimes the experimental results surpass the theoretical ones, this happens at the expense of lower fidelity of the cloning process.

5.5   Results

In order to verify the versatile nature of the cloner, we performed a series of measurements in three regimes: PCC, MPCC, and UC. These regimes differ just in the amount of *a priori* knowledge about the cloned state. For the PCC and MPCC we verified the theoretical prediction of maximally achievable average fidelity as a function of polar angle θ. For all polar angles (except the poles) we estimated the fidelities of both clones for four different equally distributed input states. The observed values are depicted in fig. 5.2 and summarised in table 5.1 for the PCC and similarly in fig. 5.3 and table 5.2 for the MPCC regime. For UC we cloned six input states: horizontally, vertically, right and left circularly, diagonally and anti-diagonally polarised states. The average fidelity obtained in UC mode is 81.5±1.2%. The vast majority of the experimentally obtained fidelities in all regimes reached or surpassed 97.5% of its theoretical prediction leading only to a very small experimental error.

Additional measurement of success probability was performed for the case of MPCC. The success probability as a function of polar angle θ is depicted in fig. 5.4. Note that success probability strongly depends on the splitting ratio of the beam splitter. Its theoretical prediction is given by

$$P_{\text{th}} = (1 - 2\mu)^2/2 + \mu\nu\tau\kappa, \tag{5.9}$$

where $\kappa = (2\mu - 1)/(1 - 2\nu)$. The presented theoretical value is therefore calculated for the above-mentioned transmittances of the beam splitter used. In order to determine the success probability of the scheme we measured the coincidence rate of the setup set to perform MPCC and also the calibration coincidence rate (all the filters were removed and the beam splitter was shifted out so that the reflected beam is no longer coupled). The ratio of these two rates determines the success probability calibrated for "technological losses" (inherent losses due to back-reflection or systematic error of all the components) [A5].

5.6   Conclusions

Our implementation presents a novel concept of multifunctional cloner optimized for quantum communication purposes with respect to *a priori* informa-

tion about transmitted states and communication channels. We have experimentally verified the versatile nature of the proposed cloner. It performs at about 97.5% of the theoretical limit for all three regimes tested (UC, PCC and MPCC). Thus, in contrast to previous implementations, it can be used in attacks against a variety of quantum cryptographic protocols at once [111]. Some of its capabilities cannot even be provided by any previous cloners especially for communication through the Pauli damping channels. Potential applications of our approach can also include practical quantum networks based on state-dependent photonic multipliers or amplifiers. We therefore conclude that this device can be an efficient tool for a large set of quantum communication and quantum engineering applications requiring cloning.

Chapter 6

Conclusions

Quantum information processing is a perspective domain of research that would hopefully some day enrich our lives with its inventions such as faster computing or unconditionally secure communications. It has already witnessed an important development over the past decades. Several important results like quantum teleportation or quantum cryptography have been accomplished both theoretically and experimentally. There is however a lot yet to be done in order to transfer this research from theoreticians' desks and experimentalists' laboratories to practical life.

This thesis presents three original QIP experiments with the ambition of contributing to the above introduced field of science. These three experiments share two major common characteristics. Firstly, the selected physical platform for all of them is linear optics. This is the reason why the second chapter discusses appropriate methods and tools of linear optics. Another common property is the number of qubits involved which is two. Although that might seam limiting, one can prove that single and two-qubit quantum gates are sufficient for universal quantum computing.

The first experiment, presented in chapter 3, successfully achieved generating two-photon Knill-Laflamme-Milburn (KLM) states. These states are known to have the capability of increasing success probability of QIP devices and therefore improve their scalability. The procedure presented in the experiment employs a tunable beam splitter to implement variable coupling ratio at the expense of introducing losses. This can in principle be overcome by using a specially designed beam splitter with preset splitting ratio suitable for specific

KLM state generation. The scheme can therefore become deterministic in the sense that it does not require any lossy transformation or post-selection which makes it suitable for a large variety of QIP devices.

Chapter four discusses the second experiment dedicated to linear-optical implementation of optimal tunable controlled phase (c-phase) gate. The c-phase gate is a two-qubit quantum device that imposes a phase shift on signal qubit conditionally if the control qubit is in logical state "1". Implementation presented in this thesis has two important qualities. First of all, the phase shift imposed by the gate can be tuned just by the choice of parameters set on employed optical components. Second major quality of this implementation is that for every phase shift it performs at maximum success probability allowed by linear optics (without additional photon ancillae). This is the motivation for performing experimental verification of maximum success probability as a function of imposed phase shift which is quite surprisingly non-monotonous.

The last experiment is presented in chapter five. In this case an optimal linear-optical multifunctional quantum cloner is discussed. In contrast to previous quantum cloners, this implementation allows to operate the device in multiple cloning regimes such as universal cloning, phase covariant cloning and mirror-phase covariant cloning. The specific *a priory* information about the cloned state is used for appropriate setting of optical components. For all of the above mentioned regimes, the device yields clones with maximum achievable fidelity. This experiment is also the first ever introduction of experimental mirror-phase covariant cloning. In this case not only the fidelity of the clones is studied but also the achievable success probability as a function of the cloned states.

Besides the three presented experiments, the author of this thesis has contributed to QIP by several other theoretical and experimental publications. He would like to express his wishes to continue in this work. There is a lot of interesting topics related to the performed experiments that are worthy further research. These topics include useful applications of the implemented c-phase gate or further investigation of the capabilities of multifunctional quantum cloning.

Shrnutí práce

Kvantové zpracování informace je perspektivní oblast výzkumu, která, doufejme, v budoucnu obohatí náš život o rychlejší výpočetní algoritmy nebo o bezpodmínečně bezpečnou komunikaci. Během uplynulých desetiletí zaznamenalo kvantové zpracování informace výrazný pokrok. Bylo dosaženo některých klíčových výsledků v teoretickém i experimentálním bádání, jako jsou například kvantová teleportace nebo kvantová kryptografie. I přes to však stále zbývá mnoho úkolů, které je nutné splnit, než se výsledky kvantového zpracování informace budou moci přenést ze stolů teoretiků nebo z laboratoří experimentátorů do běžného života.

Tato práce představuje tři původní kvantově informační experimenty s cílem přispět k výzkumu v této oblasti. Všechny tři experimenty spojují dvě základní společné vlastnosti. Zaprvé všechny experimenty jsou postavené na platformě lineární optiky. Z tohoto důvodu práce ve druhé kapitole popisuje potřebné metody a nástroje lineární optiky. Druhým společným rysem je použitý počet fotonů, který je dva. I přes to, že se tento počet může zdát nízký, je možné dokázat, že jakékoliv optické kvantově informační zařízení lze sestavit zřetězením jedno a dvou qubitových hradel.

V prvním experimentu, představeném ve třetí kapitole, jsme úspěšně dosáhli generace tzv. Knillových-Laflammových-Milburnových (KLM) stavů. Tyto stavy umožňují v principu výrazným způsobem zvýšit účinnost kvantově optického počítání. To by dovolovalo sestavit ze základních hradel složitější výpočetní celky. Popsaný experiment využívá posuvného děliče svazku a tím dosahuje laditelného dělicího poměru za cenu ztrát. Principiálně je však možné tento dělič nahradit speciálním děličem s předem nastaveným dělicím poměrem vhodným pro přípravu požadovaného KLM stavu. S touto modifikací se schéma stává zcela deterministické v tom smyslu, že nepotřebuje provádět žádné ztrá-

tové transformace nebo post-selekci. Tím se stává vhodným pro širokou škálu kvantově informačních zařízení.

Kapitola čtyři představuje druhý experiment zabývající se sestavením optimálního laditelného hradla pro podmíněnou změnu fáze (tzv. *controlled phase*). Toto dvouqubitové hradlo změní fázi mezi logickým stavem „0“ a „1“ u signálního qubitu podmíněně podle stavu kontrolního qubitu. Důležité je zmínit dvě hlavní přednosti naší implementace tohoto hradla. Fáze, kterou hradlo vnáší, je zcela libovolně nastavitelná v celém intervalu $[0, \pi]$. Navíc pro všechny nastavené fáze pracuje hradlo s nejvyšší možnou pravděpodobností úspěchu, které lze dosáhnout s využitím lineární optiky (bez nutnosti přidávat pomocné fotony). Významným výsledkem tohoto experimentu bylo ověření průběhu pravděpodobnosti úspěchu tohoto hradla v závislosti na nastavené fázi, který je překvapivě nemonotónní.

Poslední experiment, zmíněný v páté kapitole, se zabývá problematikou kvantového kopírování. Oproti předchozím kvantovým klonerům umožňuje zde představené zařízení kopírovat kvantové stavy v několika významných režimech, jako jsou univerzální klonování, fázově kovariantní klonování a zrcadlové fázově kovariantní klonování. Předem známá informace o kopírovaném kvantovém stavu je využita k nastavení optických komponent. Zařízení pak kopíruje kvantové stavy s maximální možnou věrností, které lze dosáhnout v rámci zákonů kvantové fyziky. Tento experiment je navíc prvním, který představil zrcadlové fázově kovariantní klonování. U tohoto režimu nebyla studována pouze věrnost získaných kopií kvantového stavu, ale také pravděpodobnost úspěchu kopírovací procedury.

Kromě výše uvedených experimentů publikoval autor této práce také několik dalších teoretických i experimentálních prací. V této výzkumné činnosti by autor rád pokračoval i nadále. Lze nalézt celou řadu zajímavých témat souvisejících s uvedenými experimenty, které si zasluhují další výzkum. Zvláště zajímavé je další studium vlastností a využití laditelného hradla pro podmíněnou změnu fáze nebo multifunkčního kvantového kloneru.

Résumé de la thèse

Le traitement de l'information quantique est un domaine de recherche perspectif qui peut en future enrichir notre vie par ses inventions comme les algorithmes de computation plus rapides ou la communication sûre. Un progrès important était déjà démontré au cours de quelques dizaines d'années. Un nombre de résultats importants était accompli théoriquement et expérimentalement comme par exemple la téléportation quantique ou la cryptographie quantique. Mais il y reste encore beaucoup de travail à faire pour transférer cette recherche des table des théoriciens et des laboratoires des chercheurs à la vie quotidienne.

Cette thèse présente trois expériences originelles sur le traitement de l'information quantique avec l'ambition de contribuer à ce champ de physique. Ces trois expériences ont deux points significatifs communs. Premièrement c'est le cadre de l'optique linéaire sur lequel ils sont tous implémentés. Pour cette raison le discours des méthodes et instruments de l'optique quantique linéaire est présenté dans le deuxième chapitre. Le deuxième point commun de ces expériences est le nombre de photons utilisés qui est deux. Même si ça pourrait sembler limitant, il est possible de démontrer que chaque appareil quantique peut être décomposé en composants mono et bi-qubit.

La première expérience, présentée dans le troisième chapitre, a réussi la préparation des états quantique de Knill, Laflamme et Milburn (KLM). Ces état sont connus pour avoir des propriétés utiles en ce qui concerne la computation quantique. En augmentant la probabilité de succès des appareils quantique, ces états permettent de rejoindre multiple appareils élémentaires en formant un appareil quantique plus complexe. Le processus de génération de ces états présentés dans ce chapitre utilise un séparateur de faisceau sur un montage de translation qui permet de changer la rapport de séparation en introduisant des

pertes. En principe ce séparateur peut être remplacé par un séparateur spécial avec le rapport de séparation choisi pour permettre la préparation d'un état KLM spécifique. Comme ça l'appareil présenté devient disant déterministe puisqu'il n'a pas besoin de transformations avec pertes ou la post-sélection ce qui le rendre utile dans un grand nombre d'applications.

Le chapitre numéro quatre discute l'implémentation optique linéaire d'un circuit quantique (*controlled-phase gate*). Ce circuit à deux qubits impose une phase entre les états logiques « 0 » et « 1 » d'un qubit signal si l'état du qubit de contrôle est « 1 ». L'implémentation décrite dans cette thèse possède deux qualités importantes. D'abord la phase imposée par le circuit peut être réglée dans l'intervalle $[0, \pi]$. Ensuite pour chaque valeur de la phase, le circuit donne la probabilité de succès maximale possible dans le cadre de l'optique linéaire (sans photons additionnels). Celui-ci nous a motivé pour étudier la relation entre la phase et la probabilité de succès qui est étonnamment non-monotone.

La dernière expérience est présentée dans le chapitre cinq. Il s'agit d'un appareil d'optique linéaire multifonctionnel à cloner des états quantiques de la manière optimale. En comparaison avec les cloneurs déjà existants, celui-ci est capable de fonctionner en multiple régimes: cloneur universel, cloneur phase-covariant et cloneur miroir phase-covariant. L'information sur l'état cloné connue *a priory* est utilisée pour régler cet appareil. En tous les régimes mentionnés, ce cloner fabrique des copies de fidélité maximale possible dans le cadre de physique quantique. Pour la première fois, cette expérience a démontrée le cloneur miroir phase-covariant. Pour cette raison on n'étudie pas seulement la fidélité des copies, mais aussi la probabilité de succès de notre appareil en fonction de l'état cloné.

À part des articles sur la recherche décrite ici en détail, l'auteur de cette thèse a publié aussi quelques autres articles théoriques et expérimentals sur la problématique du traitement de l'information quantique. Il veut exprimer son désir de continuer ce travail. Il y a beaucoup de sujet proches aux expériences décrites suffisamment intéressants pour constituer l'avenir de sa recherche. Ces sujet contient par exemple les applications des circuits construits ou les capacité du cloneur multifonctionnel.

Author's publications

[A1] K. Lemr, A. Černoch, J. Soubusta, and J. Fiurášek, *"Experimental preparation of two-photon Knill-Laflamme-Milburn states,"* Phys. Rev. A **81** (1), 012321 (2010).

[A2] K. Lemr, *"Preparation of Knill–Laflamme–Milburn states using a tunable controlled phase gate,"* Journal of Physics B: Atomic, Molecular and Optical Physics **44**, 195501 (2011).

[A3] K. Lemr and J. Fiurášek, *"Preparation of entangled states of two photons in several spatial modes,"* Phys. Rev. A **77** (2), 023802 (2008).

[A4] K. Lemr, *"Generation of higly non-classical states of light and atoms,"* Master's thesis, Palacký University in Olomouc (2008).

[A5] K. Lemr, A. Černoch, J. Soubusta, K. Kieling, J. Eisert, and M. Dušek, *"Experimental implementation of the optimal linear-optical controlled phase gate,"* Phys. Rev. Lett. **106** (1), 13602 (2011).

[A6] K. Lemr, K. Bartkiewicz, A. Černoch, J. Soubusta, and A. Miranowicz, *"Experimental linear-optical implementation of a multi functional optimal cloner,"* submitted, arXiv:1201.6234.

[A7] K. Lemr and J. Fiurášek, *"Conditional preparation of arbitrary superpositions of atomic Dicke states,"* Phys. Rev. A **79** (4), 043808 (2009).

[A8] E. Halenková, A. Černoch, K. Lemr, J. Soubusta, and S. Drusová, *"Experimental implementation of the multifunctional compact two-photon state analyzer,"* Appl. Opt. **51** (4), 474–478 (2012).

[A9] K. Lemr, *"Využití open source v laboratoři kvantové optiky,"* Open-Magazin **1/2010**, 19–21 (2010).

[A10] A. Černoch, O. Haderka, E. Halenková, M. Hamar, D. Javůrek, K. Lemr,
       R. Machulka, V. Michálek, J. Peřina, J. Soubusta, and J. Svozilík,
       "Experimentální kvantová optika ve Společné laboratoři optiky," Jemná
       mechanika a optika **1/2012**, 16–20 (2012).

References

[1] E. Schrödinger, *"Die gegenwärtige Situation in der Quantenmechanik,"* Naturwissenschaften **23** (49), 823–828 (1935).

[2] M. Planck, *"Entropy and Temperature of Radiant Heat,"* Annalen der Physik **1**, 719–737 (1900).

[3] R. P. Feynman, R. B. Leighton, and M. Sands, *The Feynman Lectures on Physics.* Addison Wesley Longman Inc. 6th ed. (1977).

[4] M. Dušek, *Koncepční otázky kvantové teorie.* Univerzita Palackého (2002).

[5] M. Kleespies, *A Short History of Radiation Theoreis - What Do They Reveal About "Antropogenic Global Warming"?* Principia Scientific International (2011).

[6] M. Planck, *"On the theory of thermal radiation,"* Annalen der Physik **4**, 553–563 (1901).

[7] J. J. Sakurai, *Modern Quantum Mechanics.* Addison-Wesley Publishing Company, Inc. revised ed. (1994).

[8] W. Gerlach and O. Stern, *"Der experimentelle Nachweis der Richtungsquantelung im Magnetfeld,"* Zeitschrift für Physik A Hadrons and Nuclei **9** (1), 349–352 (1922).

[9] H. Hertz, *"Ueber sehr schnelle electrische Schwingungen,"* Annalen der Physik **267** (7), 421–448 (1887).

[10] G. Marconi, *"Wireless telegraphy,"* Journal of the Institution of Electrical Engineers **28** (139), 273–290 (1899).

[11] *"Worldwide mobile cellular subscribers to reach 4 billion mark late 2008,"* tech. rep. International Telecommunication Union Geneva (2008).

[12] B. Yurke, *"Input States for Enhancement of Fermion Interferometer Sensitivity,"* Phys. Rev. Lett. **56**, 1515 (1986).

[13] M. Hillery and L. Mlodinow, *"Interferometers and minimum-uncertainty states,"* Phys. Rev. A **48**, 1548 (1993).

[14] C. Brif and A. Mann, *"Nonclassical interferometry with intelligent light,"* Phys. Rev. A **54**, 4505 (1996).

[15] J. Dowling, *"Correlated input-port, matter-wave interferometer: Quantum-noise limits to the atom-laser gyroscope,"* Phys. Rev. A **57**, 4736 (1998).

[16] K. J. Resch, K. L. Pregnell, R. Prevedel, A. Gilchrist, G. J. Pryde, J. L. O'Brien, and A. G. White, *"Time-Reversal and Super-Resolving Phase Measurements,"* Phys. Rev. Lett. **98** (22), 223601 (2007).

[17] A. Boto, P. Kok, D. Abrams, S. Braunstein, C. Williams, and J. Dowling, *"Quantum Interferometric Optical Lithography: Exploiting Entanglement to Beat the Diffraction Limit,"* Phys. Rev. Lett. **85**, 2733 (2000).

[18] G. Bjork, L. Sanchez-Soto, and J. Soderholm, *"Entangled-State Lithography: Tailoring Any Pattern with a Single State,"* Phys. Rev. Lett. **86**, 4516 (2000).

[19] M. D'Angelo, M. Chekhova, and Y. Shih, *"Two-Photon Diffraction and Quantum Lithography,"* Phys. Rev. Lett. **87**, 013602 (2001).

[20] M. Nielsen and I. Chuang, *Quantum Computation and Quantum Information.* Cambridge: Cambridge University Press (2002).

[21] D. Deutsh and R. Jozsa, *"Rapid solutions of problems by quantum computation,"* in *Proc. Roy. Soc. London Ser. A* **439**, 553–558, (1992).

[22] P. W. Shor, *"Polynomial-Time Algorithms for Prime Factorization and Discrete Logarithms on a Quantum Computer,"* SIAM J. Sci. Statist. Comput. **26**, 1484 (1997).

[23] A. Ekert and R. Jozsa, *"Quantum computation and Shor's factoring algorithm,"* Rev. Mod. Phys. **68** (3), 733–753 (1996).

[24] L. M. K. Vandersypen, M. Steffen, G. Breyta, C. S. Yannoni, M. H. Sherwood, and I. Chuang, *"Experimental realization of Shor's quantum factoring algorithm using nuclear magnetic resonance,"* Nature (London) **414**, 883–887 (2001).

[25] C. Lu, D. Browne, T. Yang, and J. Pan, *"Demonstration of a compiled version of Shor's quantum factoring algorithm using photonic qubits,"* Phys. Rev. Lett. **99** (25), 250504 (2007).

[26] C. Benett and G. Brassard, *"Quantum Cryptography: Public key distribution and coin tossing,"* in *IEEE International Conference on Computers, Systems, and Signal Processing* 175, (1984).

[27] C. Benett, F. Bessette, G. Brassard, L. Salvail, and J. Smolin, *"Experimental Quantum Cryptography,"* Journal of Cryptology **5** (1), 3–28 (1992).

[28] A. K. Ekert, *"Quantum cryptography based on Bell's theorem,"* Phys. Rev. Lett. **67** (6), 661–663 (1991).

[29] N. Gisin, G. Ribordy, W. Tittel, and H. Zbinden, *"Quantum cryptography,"* Rev. Mod. Phys. **74** (1), 145–195 (2002).

[30] T. C. Ralph, *"Continuous variable quantum cryptography,"* Phys. Rev. A **61** (1), 010303 (1999).

[31] S. F. Pereira, Z. Y. Ou, and H. J. Kimble, *"Quantum communication with correlated nonclassical states,"* Phys. Rev. A **62** (4), 042311 (2000).

[32] J. M. Renes, *"Equiangular spherical codes in quantum cryptography,"* Quantum Information & Computation **5** (1), 81–92 (2005).

[33] L. Grover, *"A fast quantum mechanical algorithm for database search,"* in *Proceedings of the twenty-eighth annual ACM symposium on Theory of computing* 212–219, ACM (1996).

[34] E. Knill, R. Laflamme, and G. Milburn, *"A scheme for efficient quantum computation with linear optics,"* Nature (London) **409**, 46 (2001).

[35] W. J. Munro, K. Nemoto, T. P. Spiller, S. D. Barrett, P. Kok, and R. G. Beausoleil, *"Efficient optical quantum information processing,"* J. Opt. B: Quantum Semiclass. Opt. **7**, S135 (2005).

[36] J. L. O'Brien, *"Optical quantum computing,"* Science **318** (5856), 1567 (2007).

[37] I. A. Walmsley, *"Looking to the future of quantum optics,"* Science **319** (5867), 1211 (2008).

[38] M. Aspelmeyer and J. Eisert, *"Quantum mechanics: Entangled families,"* Nature **455** (7210), 180–181 (2008).

[39] A. Politi, M. J. Cryan, J. G. Rarity, S. Yu, and J. L. O'Brien, *"Silica-on-silicon waveguide quantum circuits,"* Science **320** (5876), 646 (2008).

[40] B. J. Smith, D. Kundys, N. Thomas-Peter, P. G. R. Smith, and I. A. Walmsley, *"Phase-controlled integrated photonic quantum circuits,"* Opt. Express **17** (16), 13516–13525 (2009).

[41] A. Černoch, *Experimentální přenos a zpracování kvantové informace v podobě polarizačního stavu fotonu.* Ph.D. thesis, Palacký University in Olomouc (2006).

[42] J. Soubusta, *Využití sestupné frekvenční parametrické konverze v optických experimentech.* assoc. professor's thesis, Palacký University in Olomouc (2009).

[43] J. D. Franson, M. M. Donegan, and B. C. Jacobs, *"Generation of entangled ancilla states for use in linear optics quantum computing,"* Phys. Rev. A **69** (5), 052328 (2004).

[44] *"Our choice from the recent literature,"* Nat. Photon. **4** (4), 196–197 (2010).

[45] K. Kieling, J. L. O'Brien, and J. Eisert, *"On photonic controlled phase gates,"* New Journal of Physics **12**, 013003 (2010).

[46] W. K. Zurek and W. H. Wooters, *"A single quantum cannot be cloned,"* Nature **299** (802), 66 (1982).

[47] V. Bužek and M. Hillery, *"Quantum copying: Beyond the no-cloning theorem,"* Phys. Rev. A **54** (3), 1844 (1996).

[48] K. Bartkiewicz, A. Miranowicz, and Ş. K. Özdemir, *"Optimal mirror phase-covariant cloning,"* Phys. Rev. A **80** (3), 032306 (2009).

[49] K. Bartkiewicz and A. Miranowicz, *"Optimal cloning of qubits given by an arbitrary axisymmetric distribution on the Bloch sphere,"* Phys. Rev. A **82** (4), 042330 (2010).

[50] M. O. Scully and M. S. Zubairy, *Quantum Optics.* Cambridge University Press (1997).

[51] J. Peřina, *Quantum Statistics of Linear and Nonlinear Optical Phenomena.* Informatorium 2nd ed. (1991).

[52] B. Thidé, *Electromagnetic field theory.* Uppsala: Upsilon Books (2004).

[53] W. R. Hamilton, *"On a general method in dynamics,"* Philosophical Transactions of the Royal Society **2**, 247–308 (1834).

[54] J. Horský, J. Novotný, and M. Štefaník, *Mechanika ve fyzice.* Academia (2001).

[55] S. L. Braunstein and P. van Loock, *"Quantum information with continuous variables,"* Reviews of Modern Physics **77** (2), 513 (2005).

[56] P. A. M. Dirac, *The Principles of Quantum Mechanics.* Oxford: Clarendon (1958).

[57] C. E. Shannon, *"A mathematical theory of Communication,"* The Bell system technical journal **27**, 379–423 (1948).

[58] B. Schumacher, *"Quantum coding,"* Phys. Rev. A **51** (4), 2738–2747 (1995).

[59] J. Heersink, C. Marquardt, R. Dong, R. Filip, S. Lorenz, G. Leuchs, and U. L. Andersen, *"Distillation of Squeezing from Non-Gaussian Quantum States,"* Phys. Rev. Lett. **96** (25), 253601 (2006).

[60] D. Bouwmeester, J. Pan, K. Mattle, M. Eibl, H. Weinfurter, and A. Zeilinger, *"Experimental quantum teleportation,"* Nature (London) **390**, 575 (1997).

[61] J.-W. Pan, S. Gasparoni, R. Ursin, G. Weigh, and A. Zeilinger, *"Experimental entanglement purification of arbitrary unknown states,"* Nature (London) **423**, 417 (2003).

[62] S. Gasparoni, J. Pan, P. Walther, T. Rudolph, and A. Zeilinger, *"Realization of a Photonic Controlled-NOT Gate Sufficient for Quantum Computation,"* Phys. Rev. Lett. **93**, 020504 (2004).

[63] M. Mohseni, A. M. Steinberg, and J. A. Bergou, *"Optical realization of optimal unambiguous discrimination for pure and mixed quantum states,"* Phys. Rev. Lett. **93**, 200403 (2004).

[64] L. Bartůšková, A. Černoch, R. Filip, J. Fiurášek, J. Soubusta, and M. Dušek, *"Optical implementation of the encoding of two qubits to a single qutrit,"* Phys. Rev. A **74** (2), 022325 (2006).

[65] M. Barbieri, C. Cinelli, P. Mataloni, and F. D. Martini, *"Polarization-momentum hyperentangled states: Realization and characterization,"* Phys. Rev. A **72** (5), 052110 (2005).

[66] A. Mair, A. Vaziri, G. Weihs, and A. Zeilinger, *"Entanglement of the orbital angular momentum states of photons,"* Nature **412** (6844), 313–316 (2001).

[67] S. P. Walborn, A. N. de Oliveira, R. S. Thebaldi, and C. H. Monken, *"Entanglement and conservation of orbital angular momentum in spontaneous parametric down-conversion,"* Phys. Rev. A **69** (2), 023811 (2004).

[68] J. T. Barreiro, T.-C. Wei, and P. G. Kwiat, *"Remote Preparation of Single-Photon "Hybrid" Entangled and Vector-Polarization States,"* Phys. Rev. Lett. **105** (3), 030407 (2010).

[69] M. Dušek, O. Haderka, and M. Hendrych, *"Application of quantum key distribution for mutual identification - experimental realization,"* Acta Physica Slovaca **48**, 169 (1998).

[70] I. Marcikic, H. de Riedmatten, W. Tittel, H. Zbinden, M. Legré, and N. Gisin, *"Distribution of Time-Bin Entangled Qubits over 50 km of Optical Fiber,"* Phys. Rev. Lett. **93** (18), 180502 (2004).

[71] R. W. Boyd, *Nonlinear optics.* Academic Press (2003).

[72] A. Černoch, J. Soubusta, L. Bartůšková, M. Dušek, and J. Fiurášek, *"Experimental implementation of partial symmetrization and anti-symmetrization of two-qubit states,"* New Journal of Physics **11**, 023005 (2009).

[73] P. G. Kwiat, E. Waks, A. G. White, I. Appelbaum, and P. H. Eberhard, *"Ultrabright source of polarization-entangled photons,"* Phys. Rev. A **60** (2), R773–R776 (1999).

[74] B. E. A. Saleh, M. C. Teich, and B. E. Saleh, *Fundamentals of photonics.* Wiley Online Library (1991).

[75] A. Černoch, L. Bartůšková, J. Soubusta, M. Ježek, J. Fiurášek, and M. Dušek, *"Experimental phase-covariant cloning of polarization states of single photons,"* Phys. Rev. A **74** (4), 042327 (2006).

[76] M. Miková, H. Fikerová, I. Straka, M. Mičuda, J. Fiurášek, M. Ježek, and M. Dušek, *"Increasing efficiency of a linear-optical quantum gate using electronic feed-forward,"* Phys. Rev. A **85** (1), 012305 (2012).

[77] G. Rieke, *Detection of Light: from the Ultraviolet to the Submillimeter.* Cambridge Univ. Press (2003).

[78] J. Řeháček, Z. Hradil, O. Haderka, J. Peřina, and M. Hamar, *"Multiple-photon resolving fiber-loop detector,"* Phys. Rev. A **67** (6), 061801 (2003).

[79] M. Ježek, J. Fiurášek, and Z. Hradil, *"Quantum inference of states and processes,"* Phys. Rev. A **68** (1), 012305 (2003).

[80] M. Paris and J. Řeháček, *Quantum State Estimation.* Springer, Berlin (2004).

[81] A. Jamiołkowski, *"Linear transformations which preserve trace and positive semidefiniteness of operators,"* Reports on Mathematical Physics **3** (4), 275–278 (1972).

[82] M. Choi, *"Completely positive linear maps on complex matrices,"* Linear algebra and its applications **10** (3), 285–290 (1975).

[83] J. Fiurášek and Z. Hradil, *"Maximum-likelihood estimation of quantum processes,"* Phys. Rev. A **63** (2), 020101 (2001).

[84] M. F. Sacchi, *"Maximum-likelihood reconstruction of completely positive maps,"* Phys. Rev. A **63** (5), 054104 (2001).

[85] J. Modlawska and A. Grudka, *"Nonmaximally Entangled States Can Be Better for Multiple Linear Optical Teleportation,"* Phys. Rev. Lett. **100** (11), 110503 (2008).

[86] J. Franson, M. Donegan, M. Fitch, B. Jacobs, and T. Pittman, *"High-Fidelity Quantum Logic Operations Using Linear Optical Elements,"* Phys. Rev. Lett. **89**, 137901 (2002).

[87] C. Hong, Z. Ou, and L. Mandel, *"Measerement of Subpicosecond Time Intervals between Two Photons by Interference,"* Phys. Rev. Lett. **59**, 2044 (1987).

[88] G. J. Pryde, J. L. O'Brien, A. G. White, S. D. Bartlett, and T. C. Ralph, *"Measuring a photonic qubit without destroying it,"* Phys. Rev. Lett. **92** (19), 190402 (2004).

[89] B. P. Lanyon, J. D. Whitfield, G. G. Gillett, M. E. Goggin, M. P. Almeida, I. Kassal, J. D. Biamonte, M. Mohseni, B. J. Powell, M. Barbieri, A. Aspuru-Guzik, and A. G. White, *"Towards quantum chemistry on a quantum computer,"* Nature Chemistry **2** (2), 106–111 (2010).

[90] J. Eisert, K. Jacobs, P. Papadopoulos, and M. B. Plenio, *"Optimal local implementation of nonlocal quantum gates,"* Phys. Rev. A **62** (5), 052317 (2000).

[91] T. B. Pittman, M. J. Fitch, B. C. Jacobs, and J. D. Franson, *"Experimental controlled-NOT logic gate for single photons in the coincidence basis,"* Phys. Rev. A **68** (3), 032316 (2003).

[92] J. I. Cirac, W. Dür, B. Kraus, and M. Lewenstein, *"Entangling Operations and Their Implementation Using a Small Amount of Entanglement,"* Phys. Rev. Lett. **86** (3), 544–547 (2001).

[93] H. F. Hofmann and S. Takeuchi, *"Quantum phase gate for photonic qubits using only beam splitters and postselection,"* Phys. Rev. A **66** (2), 024308 (2002).

[94] N. K. Langford, T. J. Weinhold, R. Prevedel, K. J. Resch, A. Gilchrist, J. L. O'Brien, G. J. Pryde, and A. G. White, *"Demonstration of a Simple Entangling Optical Gate and Its Use in Bell-State Analysis,"* Phys. Rev. Lett. **95** (21), 210504 (2005).

[95] N. Kiesel, C. Schmid, U. Weber, R. Ursin, and H. Weinfurter, *"Linear Optics Controlled-Phase Gate Made Simple,"* Phys. Rev. Lett. **95** (21), 210505 (2005).

[96] B. P. Lanyon, M. Barbieri, M. P. Almeida, T. Jennewein, T. C. Ralph, K. J. Resch, G. J. Pryde, J. L. O/'Brien, A. Gilchrist, and A. G. White, *"Simplifying quantum logic using higher-dimensional Hilbert spaces,"* Nat. Phys. **5** (2), 134–140 (2009).

[97] J. Soubusta, L. Bartůšková, A. Černoch, J. Fiurášek, and M. Dušek, *"Several experimental realizations of symmetric phase-covariant quantum cloners of single-photon qubits,"* Phys. Rev. A **76** (4), 042318 (2007).

[98] J. F. Poyatos, J. I. Cirac, and P. Zoller, *"Complete Characterization of a Quantum Process: The Two-Bit Quantum Gate,"* Phys. Rev. Lett. **78** (2), 390–393 (1997).

[99] I. L. Chuang and M. A. Nielsen, *"Prescription for experimental determination of the dynamics of a quantum black box,"* Journal of Modern Optics **44** (11-12), 2455–2467 (1997).

[100] V. Scarani, S. Iblisdir, N. Gisin, and A. Acin, *"Quantum cloning,"* Rev. Mod. Phys. **77**, 1225–1256 (2005).

[101] N. J. Cerf and J. Fiurášek, *"Optical Quantum Cloning,"* Progress in Optics, Edt. E. Wolf (Elsevier, 2006) **49**, 455–545 (2006).

[102] M. Ricci, F. Sciarrino, C. Sias, and F. D. Martini, *"Teleportation scheme implementing contextually the Universal Optimal Quantum Cloning Machine and the Universal Not Gate. Complete experimental realization,"* Phys. Rev. Lett. **92**, 047901 (2004).

[103] W. T. Irvine, A. Lamas-Linares, M. de Dood, and D. Bouwmeester, *"Optimal Quantum Cloning on a Beam Splitter,"* Phys. Rev. Lett. **92**, 047902 (2004).

[104] I. A. Khan and J. C. Howell, *"Hong-Ou-Mandel cloning: Quantum copying without an ancilla,"* Phys. Rev. A **70** (1), 010303 (2004).

[105] H. Chen, X. Zhou, D. Suter, and J. Du, *"Experimental realization of $1 \to 2$ asymmetric phase-covariant quantum cloning,"* Phys. Rev. A **75** (1), 012317 (2007).

[106] L. Bartůšková, M. Dušek, A. Černoch, J. Soubusta, and J. Fiurášek, *"Fiber-Optics Implementation of an Asymmetric Phase-Covariant Quantum Cloner,"* Phys. Rev. Lett. **99** (12), 120505 (2007).

[107] J. Soubusta, L. Bartůšková, A. Černoch, M. Dušek, and J. Fiurášek, *"Experimental asymmetric phase-covariant quantum cloning of polarization qubits,"* Phys. Rev. A **78** (5), 052323 (2008).

[108] D. Bruß, M. Cinchetti, G. M. D'Ariano, and C. Macchiavello, *"Phase-covariant quantum cloning,"* Phys. Rev. A **62** (1), 012302 (2000).

[109] G. M. D'Ariano and C. Macchiavello, *"Optimal phase-covariant cloning for qubits and qutrits,"* Phys. Rev. A **67** (4), 042306 (2003).

[110] J. Fiurášek, *"Optical implementations of the optimal phase-covariant quantum cloning machine,"* Phys. Rev. A **67** (5), 052314 (2003).

[111] L. Gyongyosi and S. Imre, *"Efficient computational information geometric analysis of physically allowed quantum cloning attacks for quantum key distribution protocols,"* WTOC **9** (3), 165–184 (2010).

Appendix

Co-author's statement

As a co-author I, Jan Soubusta, hereby confirm that Karel Lemr provided major contribution to the experimental implementation and data processing in the following publications

- Karel Lemr, Antonín Černoch, Jan Soubusta, and Jaromír Fiurášek
  Experimental preparation of two-photon Knill-Laflamme-Milburn states
  Phys. Rev. A **81**, 012321 (2010)

- Karel Lemr, A. Černoch, J. Soubusta, K. Kieling, J. Eisert, and M. Dušek
  Experimental Implementation of the Optimal Linear-Optical Controlled Phase Gate
  Phys. Rev. Lett. **106**, 013602 (2011)

- Karel Lemr, K. Bartkiewicz, A. Černoch, J. Soubusta and A. Miranowicz
  Experimental linear-optical implementation of a multifunctional optimal cloner
  to be published

In the case of the first item, Karel Lemr also provided major contribution to the theoretical design of the experiment.

Co-author's statement

As a co-author I, Antonín Černoch, hereby confirm that Karel Lemr provided major contribution to the experimental implementation and data processing in the following publications

- Karel Lemr, Antonín Černoch, Jan Soubusta, and Jaromír Fiurášek
  Experimental preparation of two-photon Knill-Laflamme-Milburn states
  Phys. Rev. A **81**, 012321 (2010)

- Karel Lemr, A. Černoch, J. Soubusta, K. Kieling, J. Eisert, and M. Dušek
  Experimental Implementation of the Optimal Linear-Optical Controlled Phase Gate
  Phys. Rev. Lett. **106**, 013602 (2011)

- Karel Lemr, K. Bartkiewicz, A. Černoch, J. Soubusta and A. Miranowicz
  Experimental linear-optical implementation of a multifunctional optimal cloner
  to be published

In the case of the first item, Karel Lemr also provided major contribution to the theoretical design of the experiment.

17.1.2012   Antonín Čec
....

Co-author's statement

As a co-author I, Karol Bartkiewicz, hereby confirm that Karel Lemr provided major contribution to experimental implementation and data processing in the following publication
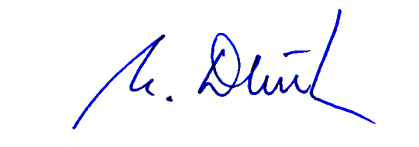
- Karel Lemr, K. Bartkiewicz, A. Černoch, J. Soubusta and A. Miranowicz
  Experimental linear-optical implementation of a multifunctional optimal cloner
  to be published

Karol Bartkiewicz

Co-author's statement

As a co-author I, Miloslav Dušek, hereby confirm that Karel Lemr provided major contribution to experimental implementation and data processing in the following publication
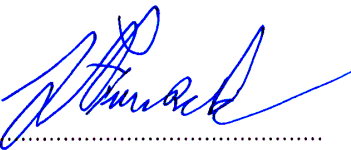
- Karel Lemr, A. Černoch, J. Soubusta, K. Kieling, J. Eisert, and M. Dušek
  Experimental Implementation of the Optimal Linear-Optical Controlled Phase Gate
  Phys. Rev. Lett. **106**, 013602 (2011)

Co-author's statement

As a co-author I, Jaromír Fiurášek, hereby confirm that Karel Lemr provided major contribution to theoretical design, experimental implementation and data processing in the following publication

- Karel Lemr, Antonín Černoch, Jan Soubusta, and Jaromír Fiurášek
  Experimental preparation of two-photon Knill-Laflamme-Milburn states
  Phys. Rev. A **81**, 012321 (2010)

....

Co-author's statement

As a co-author I, Konrad Kieling, hereby confirm that Karel Lemr provided major contribution to the experimental implementation and data processing in following publication

- Karel Lemr, A. Černoch, J. Soubusta, K. Kieling, J. Eisert, and M. Dušek
  Experimental Implementation of the Optimal Linear-Optical Controlled Phase Gate
  Phys. Rev. Lett. **106**, 013602 (2011)

....

Co-author's statement

As a co-author I, Adam Miranowicz, hereby confirm that Karel Lemr provided major contribution to experimental implementation and data processing in the following publication

- Karel Lemr, K. Bartkiewicz, A. Černoch, J. Soubusta and A. Miranowicz
  Experimental linear-optical implementation of a multifunctional optimal cloner
  to be published